NASA Technical Memorandum 101741

Multiaxis Thrust Vectoring Using Axisymmetric Nozzles and Postexit Vanes on an F/A-18 Configuration Vehicle

Albion H. Bowers, Gregory K. Noffz, Sue B. Grafton, Mary L. Mason, and Lee R. Peron

April 1991

National Aeronautics and Space Administration

NASA Technical Memorandum 101741

Multiaxis Thrust Vectoring Using Axisymmetric Nozzles and Postexit Vanes on an F/A-18 Configuration Vehicle

Albion H. Bowers and Gregory K. Noffz
NASA Dryden Flight Research Facility, Edwards, California

Sue B. Grafton and Mary L. Mason
NASA Langley Research Center, Hampton, Virginia

Lee R. Peron
California Polytechnic State University, San Luis Obispo, California

1991

NASA
National Aeronautics and
Space Administration

Dryden Flight Research Facility
Edwards, California 93523-0273

MULTIAXIS THRUST VECTORING USING AXISYMMETRIC NOZZLES AND POSTEXIT VANES ON AN F/A-18 CONFIGURATION VEHICLE

Albion H. Bowers, Gregory K. Noffz
NASA Dryden Flight Research Facility

Sue B. Grafton, Mary L. Mason
NASA Langley Research Center
and
Lee R. Peron
California Polytechnic State University

ABSTRACT

A ground-based investigation was conducted on an operational system of multiaxis thrust vectoring using postexit vanes around an axisymmetric nozzle. This thrust vectoring system will be tested on the NASA F/A-18 High Alpha Research Vehicle (HARV) aircraft. The system provides thrust vectoring capability in both pitch and yaw. Ground-based data were gathered from two separate tests at NASA Langley Research Center. The first was a static test in the 16-ft Transonic Tunnel Cold-Jet Facility with a 14.25-percent scale model of the axisymmetric nozzle and the postexit vanes. The second test was conducted in the 30- by 60-ft wind tunnel with a 16-percent F/A-18 complete configuration model. Data from the two tests are being used to develop models of jet plume deflection and thrust loss as a function of vane deflection. In addition, an aerodynamic interaction model based on plume deflection angles will be developed. Results from the scale model nozzle test showed that increased vane deflection caused increased exhaust plume turning. Other effects that caused increased thrust vectoring with given vane deflections were (1) increasing nozzle pressure ratio, (2) decreased vane radial spacing, and (3) two-vane compared to single-vane deflections. Significant nonlinear plume deflection to vane deflection effects were also documented. Aerodynamic interaction effects consisted primarily of favorable interaction of moments and unfavorable interaction of forces caused by the vectored jet plume. Some effectiveness change was noted in the rudder control power with pitch vectoring directions. Significant nonlinearities as a function of thrust coefficient were also found.

NOMENCLATURE

Aerodynamic forces and moments on the F/A-18 High Alpha Research Vehicle Thrust Vectoring Control System (HARV TVCS) aircraft model are taken at the 0.24 chord position. Vectoring direction definitions for plume deflections are: up is negative, down is positive, right is negative, and left is positive. When the thrust vectoring vanes are not installed, the nozzle configuration is defined as unvectored. For the aerodynamic interaction tests, the plume deflections are $-17°$ up, $14°$ down, and $-9°$ right. When 2 vanes are deflected into the exhaust, for any one engine, the third vane is retracted at $-10°$ deflection and is referred to as the retracted vane.

C_D	drag force coefficient
C_L	lift force coefficient
C_Y	side force coefficient
C_ℓ	rolling moment coefficient
C_m	pitching moment coefficient
C_n	yawing moment coefficient
C_{n_β}	linearized yawing moment coefficient with β
$C_{n_\beta}\|_{\delta_r = 30}$	linearized yawing moment coefficient with β at 30° rudder deflection
C_t	thrust force coefficient
HARV	High Alpha Research Vehicle
NASA	National Aeronautics and Space Administration
NPR	nozzle pressure ratio
TVCS	Thrust Vectoring Control System
α	angle of attack, deg
β	angle of sideslip, deg
δ_a	aileron deflection, $\frac{\ell - r}{2}$, deg
δ_e	elevator deflection, deg
$\delta_{j_{rms}}$	root-mean-square jet deflection angle, deg
$\delta_{\ell ef}$	leading-edge flap deflection, deg
δ_p	pitch jet deflection angle, deg
δ_r	rudder deflection, relative to swept hingeline, deg
δ_{tef}	trailing-edge flap deflection, deg
δ_v	vane deflection, relative to the engine centerline, deg
δ_y	yaw jet deflection angle, deg

INTRODUCTION

In recent years, interest in thrust vectoring[1-2] has led to many experiments designed to incorporate thrust vectoring into current and next-generation aircraft. Most of these studies have focused on vectoring in the pitch plane to improve the pitch control power[2-3] or yaw plane to improve yaw control power.[4]

To date, no aircraft have flown with the capability of vectoring in both pitch and yaw, although two aircraft are rapidly approaching flight status with multiaxis thrust vectoring capability. These two aircraft are the Navy X-31A[5] and the NASA F/A-18 High Alpha Research Vehicle Thrust Vectoring Control System (HARV TVCS). The vectoring systems for both aircraft employ axisymmetric nozzles with postexit vanes. Based on a previous study, both aircraft employ three postexit vanes radially displaced about their axisymmetric nozzles.[6]

Early information was required to properly evaluate an axisymmetric nozzle with postexit exhaust vanes as applied to the F/A-18 HARV TVCS aircraft. The early information was provided by testing

ground-based models representative of the F/A-18 HARV TVCS. A cold-jet static (wind off) test, at the NASA Langley Research Center's 16-ft Transonic Tunnel, was used to evaluate the thrust turning effectiveness of the postexit vanes. The other test, an aerodynamic interaction test at NASA Langley's Full-Scale Facility 30- by 60-ft wind tunnel, was used to evaluate the aerodynamic interaction effects on the F/A-18 aircraft caused by vectoring the exhaust jet plume.

The tests were conducted to aid in control system design, evaluation, and simulation of the F/A-18 HARV TVCS aircraft. Test results will be used to assist in the evaluation of an operational system for installation on the F/A-18 HARV to be flown at the NASA Dryden Flight Research Facility.

This paper presents a cursory overview of the data resulting from the cold-jet and 30- by 60-ft wind-tunnel tests. Significant results, applicable to the F/A-18 HARV TVCS aircraft are discussed.

TEST EQUIPMENT

Background

The F/A-18 HARV TVCS aircraft is a high-performance twin turbofan jet engine fighter–attack airplane built by the McDonnell Douglas Corp. (St. Louis, Missouri) (Fig. 1). It has shoulder-mounted wings, twin vertical tails canted outward at 20° from the vertical, mid-mounted horizontal tailplanes and leading-edge extensions which run forward along the fuselage to near the canopy. The engines installed in this aircraft are the F404-GE-400 (General Electric, Lynn, Massachusetts) rated at 10,000 lb static sea level thrust in full military power and 16,000 lb static sea level thrust in the maximum afterburner setting.

The geometry of the TVCS hardware uses three vanes mounted around each engine of the F/A-18 aircraft. Vanes replace the standard divergent nozzle and external flaps. The convergent part of the nozzle remains on the aircraft. The vanes were designed to be stowed well out of the exhaust plume. During vectoring maneuvers a maximum of two vanes on any engine will be commanded in contact with the flow to help alleviate thermal constraints.

The nozzle area in the military power setting has an exit area of 220 in^2 on the aircraft. The maximum afterburner nozzle area is typically 348 in^2 for the thrust vectoring envelope on the aircraft, Mach 0.2 to Mach 0.7, and 15,000-ft to 35,000-ft altitude.

The vane configuration is depicted for the left engine only (Fig. 2). The upper vane centerline is 5° outboard of the vertical plane. From the upper vane centerline to the outboard vane centerline is 118°. It is 103.5° from the outboard vane centerline to the lower vane centerline and 138.5° from the lower vane centerline back to the upper vane centerline. The aircraft is symmetric about the centerline, so the right engine is a mirror image of the left engine.

The upper vane was designed as the largest of the three vanes. Figure 3 shows the relative sizes of the vanes used on the aircraft with dimensions. The exhaust plume side of each vane is radiused and concave, with each vane forming part of a spherical surface. The engine exhaust is turned by the vanes. The amount of jet exhaust turning the plume deflection, or jet turning angle, is defined as the root mean square of the equivalent thrust vector. The equivalent thrust vector deflection angle in pitch and yaw is measured by the resultant force (Fig. 4). The axial thrust loss for the deflected flow is defined as theloss in the absolute value of thrust of the axial force when compared to the absolute value of the undeflected

thrust. The normalized axial thrust is the absolute value of the axial force divided by the absolute value of the undeflected thrust.

Cold-Jet Model

The 14.25-percent scale axisymmetric model was tested in the cold-jet facility[7] at the NASA Langley Transonic Tunnel. The cold-jet standard instrumentation included a force and moment balance and pressure taps. The total and static pressures were used to determine the nozzle pressure ratio (NPR).

The single isolated nozzle was a model of the left engine. The external flow around the model nozzle was not tested in the cold-jet test, so no attempt was made to model the external geometry of the nozzle. The size of the axisymmetric nozzles used in the cold-jet test corresponded to the military power and maximum afterburner nozzle sizes (Fig. 5). The vanes in this test were also 14.25 percent of full scale. The vanes were adjusted manually and then held in place by the clamping force of the set screws. Shims were also installed to accurately position the vanes relative to the nozzle. The vane deflections in the test were set from $-10°$ to $30°$ for most conditions. The vanes were set individually by hand using protractors, resulting in the accuracy of any particular setting of vane deflection angle of closer than $\pm\frac{1}{2}°$.

Aerodynamic Interaction Wind-Tunnel Model

The aerodynamic interaction model was tested in the 30- by 60-ft wind tunnel at NASA Langley. The aerodynamic interaction part of the investigation used a 16-percent scale F/A-18 model to simulate the HARV TVCS aircraft (Fig. 6). The model, designed for use in free-flight testing, was of very light construction. The lightweight construction of the model resulted in the use of low dynamic pressures to prevent structural damage. The radial location of the vanes was oriented the same as for the cold-jet test. The hinges were located in a position that would allow correct vane position and deflection angles. The vanes were manipulated from the control station of the 30- by 60-ft wind tunnel by flexible control cables and control position transducers which indicated the vane position. A spin chute canister was also a part of the F/A-18 HARV TVCS configuration and was included in the modifications made to the model.

This particular F/A-18 model was used because it was a free-flight model that already had ducting for the inlets, exhausts, and high pressure air built into the design.[8] The primary difference between the aircraft and cold-jet configurations, and the aerodynamic interaction model configurations was the tailpipe areas. The tailpipes used in the aerodynamic interaction test (Fig. 7) were 13.31 in^2 in area, which corresponds to a 520 in^2 tailpipe area on the full-size F/A-18 aircraft. The tailpipe area used during flight tests is 348 in^2 in the thrust vectoring envelope.

Other differences existed between the flight aircraft configuration and the wind-tunnel-model configuration. One difference was that the video camera fairings were omitted on the model. Another difference was the presence of research airdata wingtip probes on the aircraft and AIM-9 missiles on the model (compare Fig. 1 to Fig. 6). In addition, the wind-tunnel configuration did not incorporate the removal of the horizontal stabilator area (1.6 percent in area) at the root-trailing-edge area that was later incorporated on the flight vehicle for thrust vectoring fairing clearance.

Cold-Jet Test Procedure

Most of the procedure involved in running the cold-jet test facility has been covered by other authors.[2,7,9] The unique aspects of the thrust vectoring concept, with postexit exhaust vanes, and its effect on the procedure will be covered briefly.

The forces and moments obtained from the force and moment balance were used to calculate the equivalent exhaust plume deflection angle. The calculated plume deflection angle, which is an indicator of the effectiveness of the system, was compared to the geometric vane deflections (δ_v).

The NPR values were selected on the basis of the expected flight NPR values with the F/A-18 HARV TVCS aircraft. The NPR varied for each configuration at values of 2, 3, 4, 5, and 6. The NPR values were repeatable to within 0.007 with the test instrumentation data.

In summary, there were over 300 configurations tested in the cold-jet test. There were two nozzle configurations, five NPRs, and different vane configurations tested (vanes off, one vane deflected, two vanes deflected, three vanes deflected, and no vanes deflected). Screening runs were also made for nozzle and vane configuration buildup.

Aerodynamic Interaction Test Procedure

The sting mount allowed angle-of-attack (α) measurements from 0° to 65° and the model was tested at 5° increments with intermediate points at 37.5° and 42.5°. Angle-of-sideslip (β) ranges were from ±30°, though most of the testing occurred at angles of +4° and −4°. The balance and structural constraints imposed by the model limited the dynamic pressure of the tunnel to 5 lb/ft^2 for the test.

For most of the tests, the horizontal stabilator was deflected at −12° and the rudders were deflected at 0°. The horizontal and rudder control powers were checked as a function of thrust vectoring direction during specific portions of the test. The leading-edge flap was always deflected to the maximum value of 34°, the trailing-edge flaps were always deflected 0°, and the ailerons were always deflected 0° for the entire test.

The thrust of the model was adjusted by changing the pressure of the air supplied to the model by its ejectors. The nominal value of the high-pressure air supplied to the model, 46 lb/in^2, resulted in a thrust coefficient of 0.8. Because of the nozzle and ejector design used in the aerodynamic interaction test the maximum NPR was approximately 1.3. The low NPR of the aerodynamic interaction test resulted in subcritical exhaust plumes which changed the relation of vane deflection to plume deflection. Because of this, the data were taken on the basis of effective plume deflection, not vane deflection. Plume deflection was determined using the wind-tunnel balance forces and moments, not by any direct method of plume deflection measurement. Using the plume deflection angle to determine aerodynamic interaction terms alleviated the effects of the subcritical exhaust plumes.

Tares are common in wind-tunnel tests and they are usually used to remove the effects of model weight. In the aerodynamic interaction test, tares were taken with the wind off and the thrust off to determine the weight tares. There were also wind-off and thrust-on tares to allow the removal of thrust effects, leaving only the aerodynamic interactions. Thrust-off runs were made to allow comparison between the baseline F/A-18 configuration and the F/A-18 HARV TVCS configuration. Thrust-on runs resulted in aerodynamic interaction effects once the thrust-on tares were used to calibrate the data.

The thrust-off runs were necessary because of the modification made to the model when the six component force and moment balance was added. A side effect of the modification was that the nozzle of the baseline F/A-18 configuration, without the HARV TVCS hardware installed, was incompatible with the internal ducting for the HARV TVCS hardware. Not having baseline F/A-18 nozzle thrust resulted in the additional requirements of runs made without power. Without a power thrust coefficient of zero, the HARV TVCS hardware was installed for direct comparison to the baseline F/A-18 nozzle configuration. This incompatibility of the internal ducting with the baseline F/A-18 configuration model resulted in two separate increments. One increment determined the effect of the HARV TVCS hardware. The other increment determined the effect of thrust vectoring.

For the tests, the thrust would be adjusted to the desired condition and the vanes deflected to give the desired degree of jet plume vectoring for a particular run. Deflecting the vanes, or vectoring, resulted in the an equivalent jet plume angle (average angle for the two plumes). Vectoring-up resulted in an equivalent effective plume turning angle of $-17°$. For vectoring-down the effective plume turning angle was 14°. For vectoring-right the equivalent effective vectoring turning angle was approximately $-9°$, averaged for both plumes.

In summary, there were 177 wind-tunnel runs made and 147 runs used the F/A-18 HARV TVCS configuration model. Of the 147 runs, 31 were wind-off tares and screening tests to determine vane effectiveness to jet plume turning. Of the 30 runs made without the F/A-18 HARV TVCS configuration, 15 were made with a baseline F/A-18 configuration.

ANALYSIS PROCEDURE

Cold-Jet Data

It was desirable to have test results for all combinations of single- and dual-vane deflections between $-10°$ and 30° at 5° increments (with intermediate data taken at 17.5° and 22.5° deflection) for each NPR. The different vane sizes and uneven radial vane spacing angles meant that there were no planes of symmetry. Therefore, each data point was unique.

Many configurations were not tested because of time constraints. The untested configurations resulted in large gaps in the desired matrix from the cold-jet test. A comprehensive test matrix was completed for the maximum afterburner nozzle configurations, and a sparse test matrix was completed for the military power nozzle configurations.

Aerodynamic Interaction Data

The data were analyzed using increments based on two different baseline configurations. The increments caused by vectoring alone were found by subtracting vectored and unvectored runs. Increments caused by the installation of the vectoring hardware were determined by subtracting TVCS hardware runs from baseline runs.

Each run was composed of a power-on tare (wind off), which was subtracted from a power-on wind-tunnel run (wind on) to remove power effects. The baseline configuration was tested first to investigate basic effects, then additional runs were made to find the effects of interest by using parametric variations. For example, power-on tare angle-of-attack sweeps of unvectored vectoring and

vectoring-down were made with the wind off. Then the same angle-of-attack sweeps were repeated with the wind on. With the wind on and calibrating the runs, by subtracting the respective tares, the thrust vectoring aerodynamic interaction terms were found. Finally, by subtracting the down-vectoring run from the unvectored run, the increment in down-vectoring down was found.

Power-off results were much easier to handle. Power-off tares are still required to remove model weight and moment forces exerted on the balance from gravity. In the cases with power off the results from the TVCS configuration would be subtracted from the baseline F/A-18 configuration to produce increments for TVCS hardware.

Control surface deflection test results would be treated the same as vectoring test results. The two results of unvectored thrust deflection with and without control surface input and vectored thrust deflection with and without control surface input would subsequently be subtracted. The final result would be the increment in control power caused by vectoring.

RESULTS AND DISCUSSION

Cold-Jet Test Results

The upper (larger) vane resulted in larger jet plume deflection angles than the lower or outer vanes by approximately 25 percent at $\delta_v = 30°$ for equal vane deflections with the military power nozzle (Fig. 8) . The vanes are intentionally stowed outside of the plume and do not become effective until the vane deflections increase above approximately 10°. The upper vane is more effective than the other 2 vanes in the maximum afterburner nozzle data (Fig. 9) as well, by approximately 50 percent in this case at $\delta_v = 30°$. With the afterburner nozzle installed, the dead band of low vane effectiveness extends out to approximately 5° vane deflection into the plume. Even though the plume begins deflecting earlier with the maximum afterburner nozzle setting, the slope is slightly lower for the maximum afterburner nozzle cases when compared to the military power nozzle cases. By the time $\delta_v = 30°$ the military power nozzle case is producing nearly the same jet plume turning angle as the maximum afterburner nozzle case.

The NPR also plays a significant part in the amount of jet plume turning angle (Fig. 10). In some cases the NPR effects are as large as 5° of equivalent plume turning angle. The dead band is affected also, though the amount is not known. The reason is that no cold-jet test data exist below the 10° vane deflection data point for the single-vane deflections with the military power nozzle cases. However, below this value of vane deflection data exist for the maximum afterburner nozzle configurations. The data shown between $-10°$ and 10° vane deflection are interpolated. The smaller dead band with higher NPRs is because of the underexpanded exhaust plume as it leaves the nozzle.

Two vanes deflected into the plume simultaneously result in plume turning effectiveness increases for a given vane deflection angle. When compared to the single vane deflections (Fig. 8), the two-vane deflections are more effective by as much as 100 percent at $\delta_v = 30°$ and an NPR = 2 (Fig. 11). The unequal vane spacing and varying vane size produced some interesting results. The upper and outer vanes produce the largest plume deflections, with the 2 small vanes producing slightly less effectiveness, by approximately 11 percent at $\delta_v = 30°$. The combination of upper and lower vanes produced the least effective plume turning by approximately 43 percent at $\delta_v = 30°$, even with the advantage of the large vane in the combination compared to the upper and outer vane combination. The results shown are at the military power nozzle setting and an NPR = 2. This is an important conclusion that radial-included angle spacing of the vanes may be as important or more important than vane size.

Two equally deflected vanes, with increasing NPR, tend to show increasing effectiveness in the data up to approximately 20° vane deflection (Fig. 12). But as the vanes deflect above this, the jet turning effectiveness decreases with increasing NPR. The decrease in plume turning angle for NPR = 6 data compared to NPR = 2 data is approximately 12 percent at $\delta_v = 30°$. The decrease in plume turning for the same vane setting is a probable result of the plume bending into the retracted vane and then straightening out toward the engine centerline again. These data are with the military power nozzle, with the two small vanes equal to each other in deflection.

The next figure (Fig. 13) shows all NPRs = 6 and with equal deflections of all two-vane combinations for the military power nozzle case. Again the two small vanes with the close radial-included angle spacing, the lower and the outer vanes, prove nearly as effective as the large upper vane in conjunction with the outer vane. The difference of the small vanes is only 11 percent at $\delta_v = 30°$, less than the upper and outer combination. Leaving the upper and lower vane combination the least effective again by approximately 60 percent at $\delta_v = 30°$ compared to the upper and outer vanes together. The turning at 30° deflection of lower and upper vanes (11.2°) results in less plume deflection than the same combination at 25° (12.5°), the retracted vane is redirecting the flow again.

The maximum afterburner nozzle is not as effective in turning the plume when compared to the military power nozzle (Fig. 14). The loss of effectiveness is evident at NPR = 2 in the upper and lower vane curve. When the maximum afterburner data are compared with the results of the military power nozzle data (Fig. 11) with both at NPR = 2 the losses of the maximum afterburner nozzle are quite large. The losses are typically between 27 percent and 37 percent at $\delta_v = 30°$. The actual turning power needs to be evaluated, as the afterburner thrust will be higher than the military power thrust and will offset the loss in plume turning effectiveness.

The lowest plume turning effectiveness is the maximum afterburner nozzle case with an NPR = 6 (Fig. 15). The maximum jet plume turning angle available is now down near 22°, as compared to a maximum of approximately 25° for NPR = 2, in the upper and outer equal vane deflection data. As the flow is deflected into the largest gap between vanes when viewed end-on, the turning effectiveness does not appear to be affected by retracted vane straightening. Plume turning in the other 2 equal-sized vane deflection cases is reduced because of possible retracted vane effects straightening out the flow above 20° vane deflection.

Thrust loss data are presented as normalized axial thrust. Increases in plume turning caused less thrust (Fig. 16). The large upper vane caused the greatest loss (0.82) at $\delta_v = 30°$, with the 2 equal-sized vanes producing nearly equal amounts of thrust loss (0.87). Results shown are for the military power nozzle case at NPR = 2.

Maximum afterburner nozzle data caused less turning for a given vane position than the military power nozzle cases. The reduced turning angles of the maximum afterburner nozzle cases compared to the military power nozzle cases also caused slightly less loss (Fig. 17) than the military power nozzle cases (Fig. 16), all other considerations being equal. With the military power nozzle at NPR = 2 for the upper vane with 30° deflection, the thrust loss was approximately 18 percent. For the same condition the maximum afterburner nozzle case was approximately 16 percent.

Comparing results from differing NPR levels caused somewhat unusual trends at high vane deflections (Fig. 18). Increasing NPR with the military power nozzle and 2-vane equal deflections show increasing levels of thrust loss up to 20° vane deflection. Above 20° vane deflection the increasing values of NPR bring less normalized axial thrust loss for most NPRs. There are two possible contributions to

this result at larger vane deflections. (1) Increasing NPR increases the size of the plume (underexpanded) and the plume impinges on more area on the vanes. This results in less exhaust plume loss through gaps between the vanes. (2) The third vane straightening effects on the exhaust plume cause an increase in the axial force.

For a fixed NPR and all combinations of two vanes deflected equally, the thrust loss was approximately the same for given vane deflections (Fig. 19). Total differences amount to less than approximately 10 percent. No observed radial-included angle vane spacing effects or differing vane size effects were found.

Using all vane combinations where at least one vane is held at 30° deflection and at least one vane is at −10° deflection results in the most extreme envelope of vectoring available (Fig. 20). This envelope is for the maximum afterburner nozzle cases with varying NPRs. Possible retracted vane effects appear at 3 of the corners: near (11, 9), (−3, −25), and (−20, 16). At the intermediate corners are the single-vane deflections which lack the possible retracted vane effects: near (−3, 18), (−10, −7), and (9, −9). The loss of effectiveness at the corners, especially near the 11° pitch and 9° yaw corner, is very apparent with increasing NPR. Loss of jet plume turning effectiveness is evident by observing the root mean square of the pitch and yaw vectoring angles decrease in magnitude with increasing NPRs. The single-vane deflection corners show that root-mean-square pitch and yaw vectoring are relatively unaffected by increases in NPR. Unlike the previous figures, Fig. 20 shows the direction in pitch and yaw, as well as the relative change in magnitude for a specific set of vane deflections.

Pitch and yaw vectoring curves for the military power nozzle configuration were determined from more limited data (Fig. 21). This resulted in more interpolation and obviously straighter lines between the corners. For the military power nozzle configuration, data were obtained only where 1 or 2 vanes were at 30° deflection. Because of NPR variation, the effects at the corners from possible retracted vane effects are just as evident as for the maximum afterburner nozzle configurations. The intermediate corners are relatively insensitive to the NPR variations as well, as seen previously in the maximum afterburner data.

Reduced vane deflections reduce the effects of the retracted third vane when presented in this vane envelope format (Fig. 22). Test results for 20° of vane deflection, military power nozzle configuration, and various NPRs show little effect of potential retracted vane effects.

Aerodynamic Interaction Test Results

Aerodynamic interaction results were analyzed as a function of equivalent plume deflection, not vane deflection, to alleviate the effects of the low NPR on the aerodynamic interaction model. Because of low NPR, the aerodynamic interaction model resulted in a subcritical exhaust, altering the vane deflection to plume deflection relationship. All thrust force and moment increments have been removed, only aerodynamic interference effects caused by vectoring remain.

The lift coefficient was affected by approximately 0.1 with vectoring (Fig. 23). This value varied slightly at the higher angles of attack. Vectoring-down caused an increase in lift coefficient (C_L), and vectoring-up the converse, such as a blown flap might produce on a wing.[10] At higher angles of attack, above the maximum C_L, vectoring-down caused a larger increase in the absolute value of lift coefficient increment from unvectored data than vectoring-up, approximately 0.10 to 0.06, respectively, at $\alpha = 55°$.

The resulting pitching moment increment was a positive moment when vectoring-up (Fig. 24) and a negative moment when vectoring-down. The vectoring-down was a favorable effect on the total moment

caused, similar to a blown flap.[10] The effects of variation in nozzle size, NPR, and Mach number were not determined from the 30- by 60-ft aerodynamic interaction tests. Because of vectoring at very high angles of attack, the pitching moment increment decreased, as did lift coefficient. The trend in pitching moment vectoring-up showed a lower increment (0.02) than vectoring-down (0.18) at high angle-of-attack values ($\alpha = 50°$). This is the same trend shown by the lift coefficient data.

All the drag test results displayed trends similar to those in Fig. 25. The drag test results shown are for a leading-edge deflection of 34°. Vectoring-down compared to unvectored vectoring caused the most drag, an increment of approximately 0.02 near $\alpha = 0°$. The amount increased to approximately 0.2 near $\alpha = 60°$, partly because of the increase in lift coefficient (Fig. 23) affecting the induced drag. Downward vectoring also may be affecting the entrained flow wake angle causing an increase in drag. Vectoring-up produces the opposite result: less drag than the unvectored data, at an increment of approximately -0.02 near $\alpha = 0°$ and increasing to approximately 0 at $\alpha = 50°$. The wind-tunnel test was not conducted to determine drag. Absolute results are less valid than the incremental trends.

When vectoring in any direction the aerodynamic increments in side force (Fig. 26) and rolling moment (Fig. 27) were smaller than the scatter. For this reason the increments caused by vectoring were set to zero. In the yawing moment data the effect of vectoring direction to the right is evident (Fig. 28). At low angles of attack (near zero) the yawing moment coefficient is 0.008 and decreases to approximately 0.003 near $\alpha = 50°$.

In the data, one unimportant aspect was the effect of the vanes alone with thrust turned off. This is illustrated (Fig. 29) in the lift coefficient data where no discernible effect could be found because of vanes alone.

Likewise, without thrust the vane deflection aerodynamic moment effects were small. For example, in the pitching moment it was found to be close to the edge of observability (Fig. 30), with increments of 0.015 or smaller. Because of noise in the signal and the increment's small size, the increment was set to zero.

The aerodynamic effect on the aircraft caused by the installation of all the vane hardware, without vane deflection on the aft end of the aircraft, was also investigated (Fig. 31). The data in lift coefficient displays little, if any, effect. Because of the baseline F/A-18 nozzle internal ducting constraints, all the data to make this comparison were taken without thrust.

In pitching moment coefficient (C_M) a small effect is seen because of thrust vectoring vane hardware installation when compared with the basic aircraft configuration (Fig. 32). The vane installation effects on pitching moment are less than 0.02 for all angles of attack tested. The net result of the installation of the HARV TVCS hardware is to make the aircraft slightly more stable than the baseline F/A-18 configuration. The F/A-18 HARV TVCS configuration was also found to be slightly more stable in yawing moment than the baseline F/A-18 configuration.

Power effects on the model aerodynamic coefficient increments were also investigated (Fig. 33). This was most evident in the directional stability as thrust coefficient was varied from 0 to 0.8. The example shown is unvectored thrust straight out of the tailpipe. The increased thrust keeps the linearized yawing moment coefficient with β (C_{n_β}) positive until $\alpha = 38°$, whereas without power it was becoming negative as low as $\alpha = 18°$. The data for C_{n_β} shown here were linearized from two angle-of-attack sweeps at $\beta = 4°$ and $\beta = -4°$. The results exhibit a marked nonlinearity with thrust variation. For much of the angle-of-attack range the increment between thrust force coefficient (C_t) = 0.0 to $C_t = 0.2$ is approximately the same magnitude as the increment between $C_t = 0.4$ to $C_t = 0.8$.

When vectoring in the pitch plane directional stability, C_{n_β} was affected slightly (Fig. 34). Below $\alpha = 40°$ the increment is difficult to see but downward vectoring usually appears as the largest increment, and above $\alpha = 40°$ it increases to as much as 0.002 when compared to unvectored vectoring. Above approximately $\alpha = 40°$, vectoring-down makes the aircraft slightly more stable than the other vectoring directions.

Finally, the only control parameter affected by vectoring thrust was the rudder power as a function of pitch vectoring (Fig. 35). Vectoring-down caused an increase in rudder control power by approximately 0.005 $C_{n_\beta}|_{\delta_r = 30}$. Rudder deflection is measured relative to the swept-rudder hingeline. This increment appears relatively constant across the angle-of-attack range with some increase above $\alpha = 50°$.

CONCLUDING REMARKS

Data are presented from two ground test investigations of an axisymmetric nozzle with postexit vanes used to vector the thrust on a F/A-18 configuration aircraft. Test results will be used to assist in the evaluation of an operational system for installation on the NASA F/A-18 High Alpha Research Vehicle (HARV).

One of the two ground-based investigations was a cold-jet test to determine the exhaust plume turning effectiveness. The cold-jet test results show that the larger vane is more effective by as much as 50 percent, with the maximum afterburner nozzle and as much as 25 percent with the military power nozzle at nozzle pressure ratio (NPR) = 2. Increases in NPR (NPR = 6) result in as much as 5° additional turning of the exhaust plume than at lower NPRs (NPR = 2) with the military power nozzle. Two vane deflections can produce as much as 100 percent more plume deflection at NPR = 2 for the military power nozzle when compared to single vane deflection test results. Potential retracted vane effects coupled with plume geometry limit the maximum plume deflections of the two vane equal deflections at higher NPRs with both the military power and the maximum afterburner nozzles. Military power nozzle test results show slightly more plume turning to vane deflection slope than maximum afterburner nozzle test results. Axial thrust loss test results from the cold-jet test showed larger losses at greater turning angles, greater losses with larger vane sizes, and greater losses in the maximum afterburner nozzle configuration when compared with the military power nozzle configuration. The vanes are stowed out of the plumes in the $-10°$ deflection position and showed no effectiveness until deflected approximately 10° into the plume.

Results from the 30- by 60-ft wind-tunnel aerodynamic interaction test showed that vectoring thrust acted like a blown flap by favorably affecting moment coefficients and unfavorably affecting force coefficients. This results in a favorable increase of up to 0.12 in pitching moment coefficient, and an approximately 0.1 decrease in lift coefficient. The results, using a low NPR of 1.3 and subcritical exhaust, were correlated with plume deflection and not vane deflection to alleviate the low NPR effects. Installation of the thrust vectoring hardware was found to slightly increase directional and pitch stability of the aircraft when compared with the directional and pitch stability of the basic aircraft configuration. A less than 10 percent increase in rudder control power was found when thrust vectoring-down in the pitch direction.

REFERENCES

[1] Capone, Francis J., and Mason, Mary L., *Multiaxis Aircraft Control Power From Thrust Vectoring at High Angles of Attack*, NASA TM-87741, 1986.

[2] Berrier, Bobby L., and Leavitt, Laurence D., *Static Internal Performance of Single-Expansion-Ramp Nozzles With Thrust-Vectoring Capability up to 60°*, NASA TP-2364, 1984.

[3] Capone, Francis J., and Berrier, Bobby L., *Investigation of Axisymmetric and Nonaxisymmetric Nozzles Installed on a 0.10-Scale F-18 Prototype Airplane Model*, NASA TP-1638, 1980.

[4] Sappington, Jeffrey W., and Thompson, LCdr Robert L., "F-14A Yaw Vane Technology Demonstration Program," 31st Symposium Proceedings, Society of Experimental Test Pilots, Sept., 1987.

[5] Lerner, Eric J., "First international X-plane to fly," *Aerospace America*, vol. 25, no. 8, 1987, pp. 6–7.

[6] Berrier, Bobby L., and Mason, Mary L., *Static Performance of an Axisymmetric Nozzle With Post-Exit Vanes for Multiaxis Thrust Vectoring*, NASA TP-2800, 1988.

[7] Mason, Mary L., and Berrier, Bobby L., *Static Performance of Nonaxisymmetric Nozzles With Yaw Thrust-Vectoring Vanes*, NASA TP-2813, 1988.

[8] Murri, Daniel G., Grafton, Sue B., and Hoffler, Keith D., *Wind-Tunnel Investigation and Free-Flight Evaluation of a Model of the F-15 STOL and Maneuver Technology Demonstrator*, NASA TP-3003, 1990.

[9] Mason, Mary L., and Berrier, Bobby L., *Static Investigation of Several Yaw Vectoring Concepts on Nonaxisymmetric Nozzles*, NASA TP-2432, 1985.

[10] Bertin, John J., and Smith, Michael L., *Aerodynamics for Engineers*, Prentice-Hall, Inc., Englewood Cliffs, NJ, 1979.

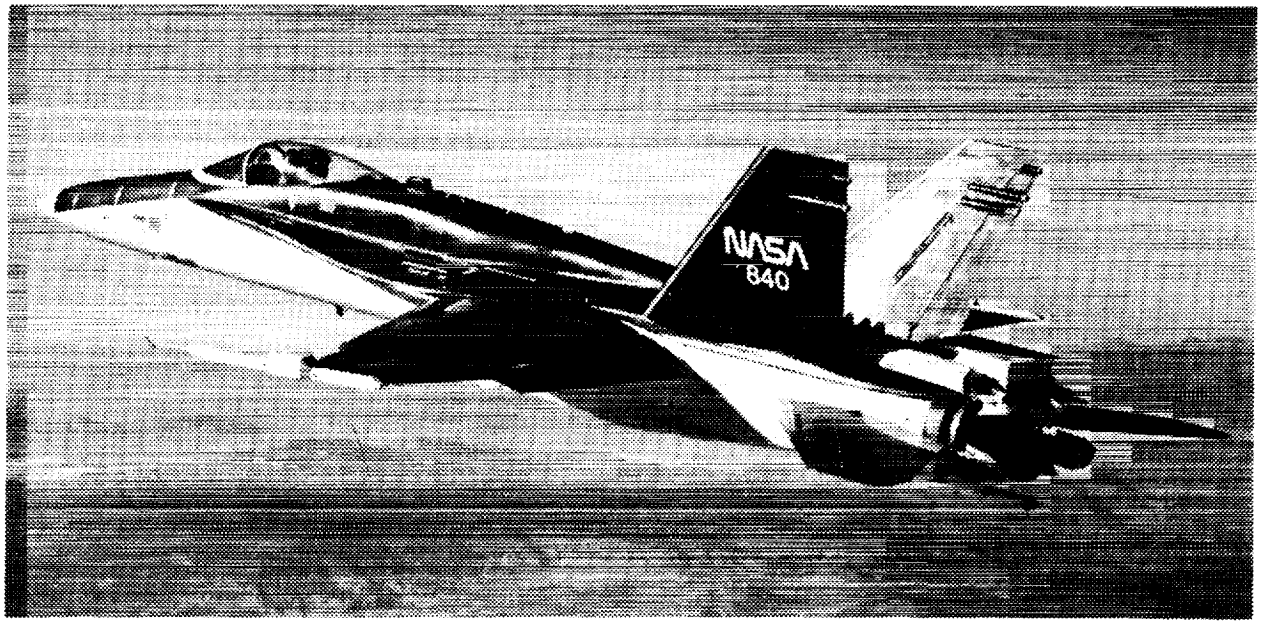

EC 910010-006

Fig. 1 The F/A-18 HARV in flight with the TVCS installed.

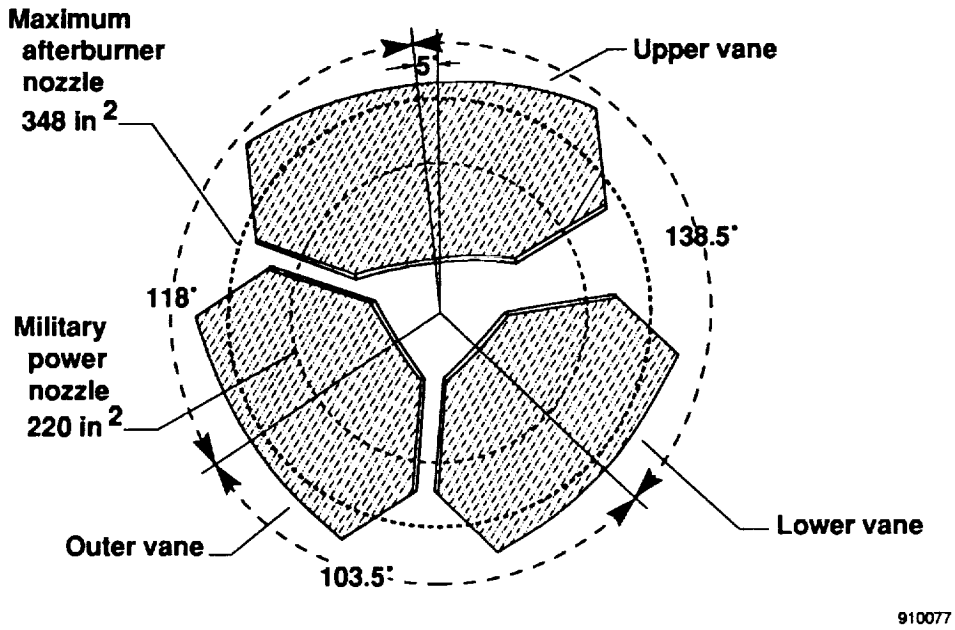

Fig. 2 Thrust vectoring control system end-view of the left engine looking forward. Radial vane included angles are displayed. All vanes shown fully extended into the plume. The right engine is a mirror image of the left.

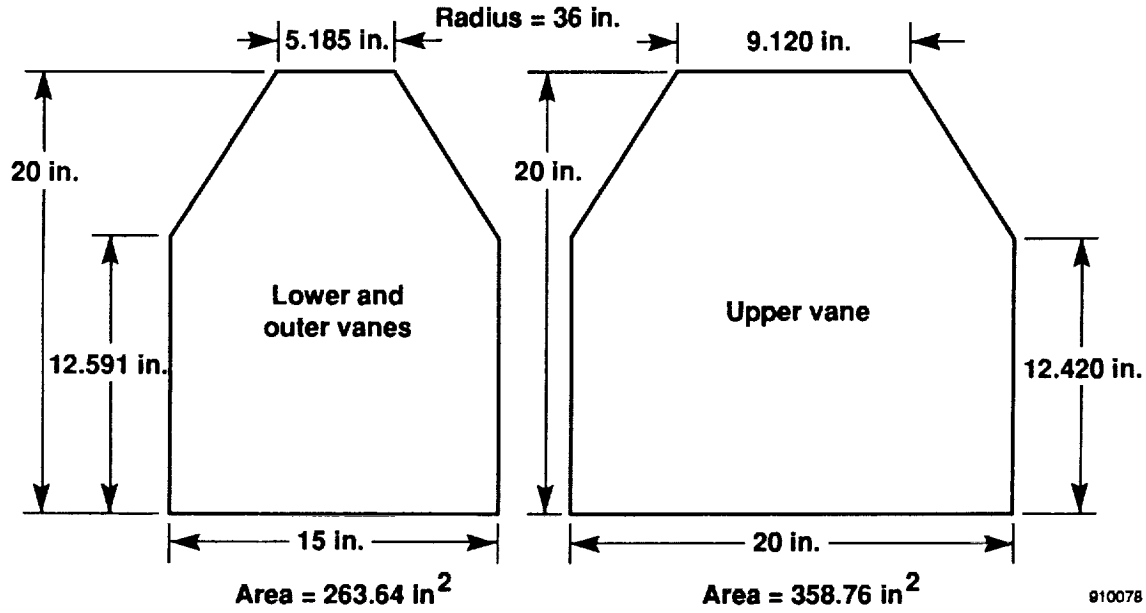

Fig. 3 Dimensions for flight vanes.

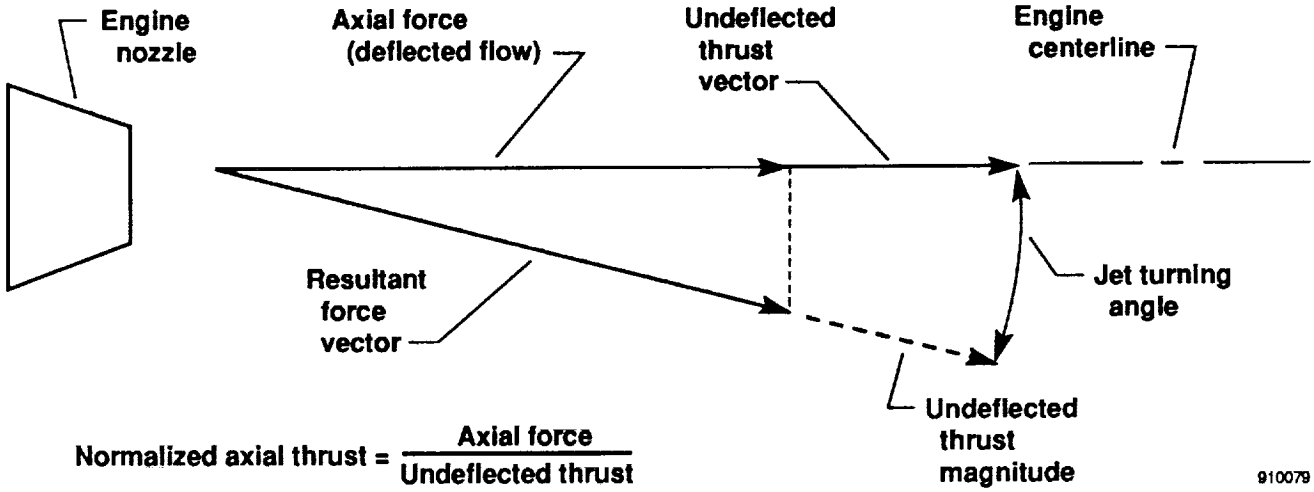

Fig. 4 Schematic of jet turning angle and axial thrust loss definitions.

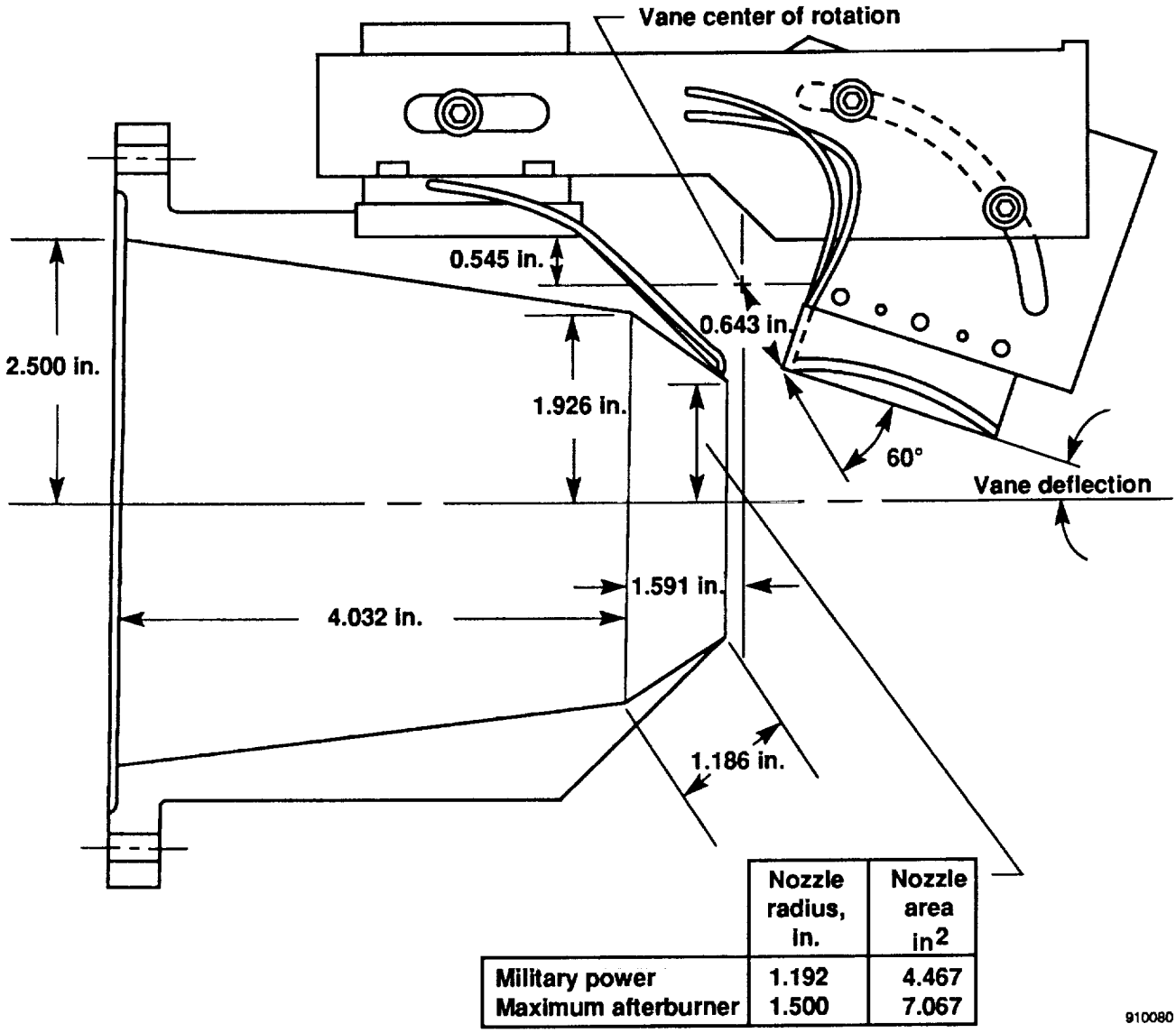

	Nozzle radius, in.	Nozzle area in^2
Military power	1.192	4.467
Maximum afterburner	1.500	7.067

Fig. 5 Detail of 14.25-percent scale model used in the cold-jet test setup. Vane center of rotation is shown.

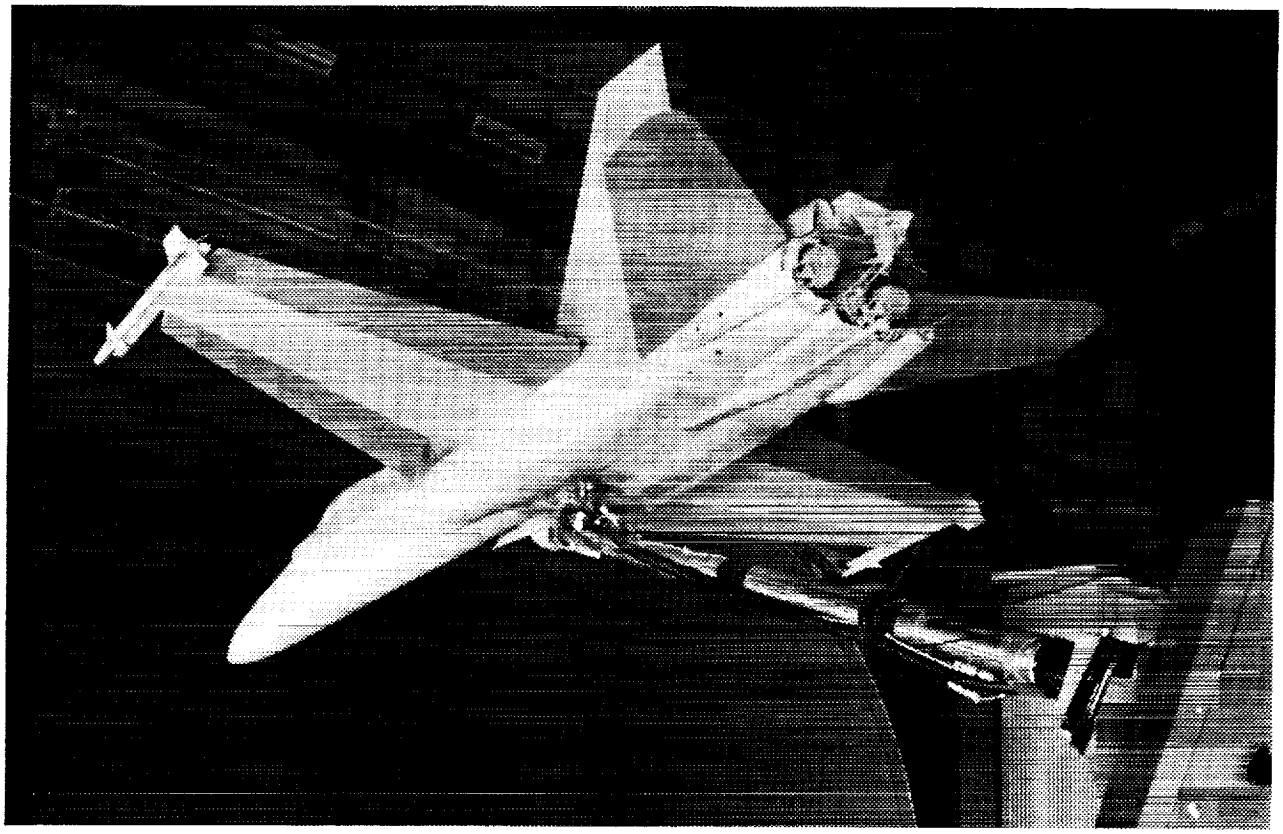

Fig. 6 F/A-18 16-percent scale model used for aerodynamic interaction testing as installed in the 30- by 60-ft wind tunnel at NASA Langley Research Center. Thrust vectoring hardware are installed.

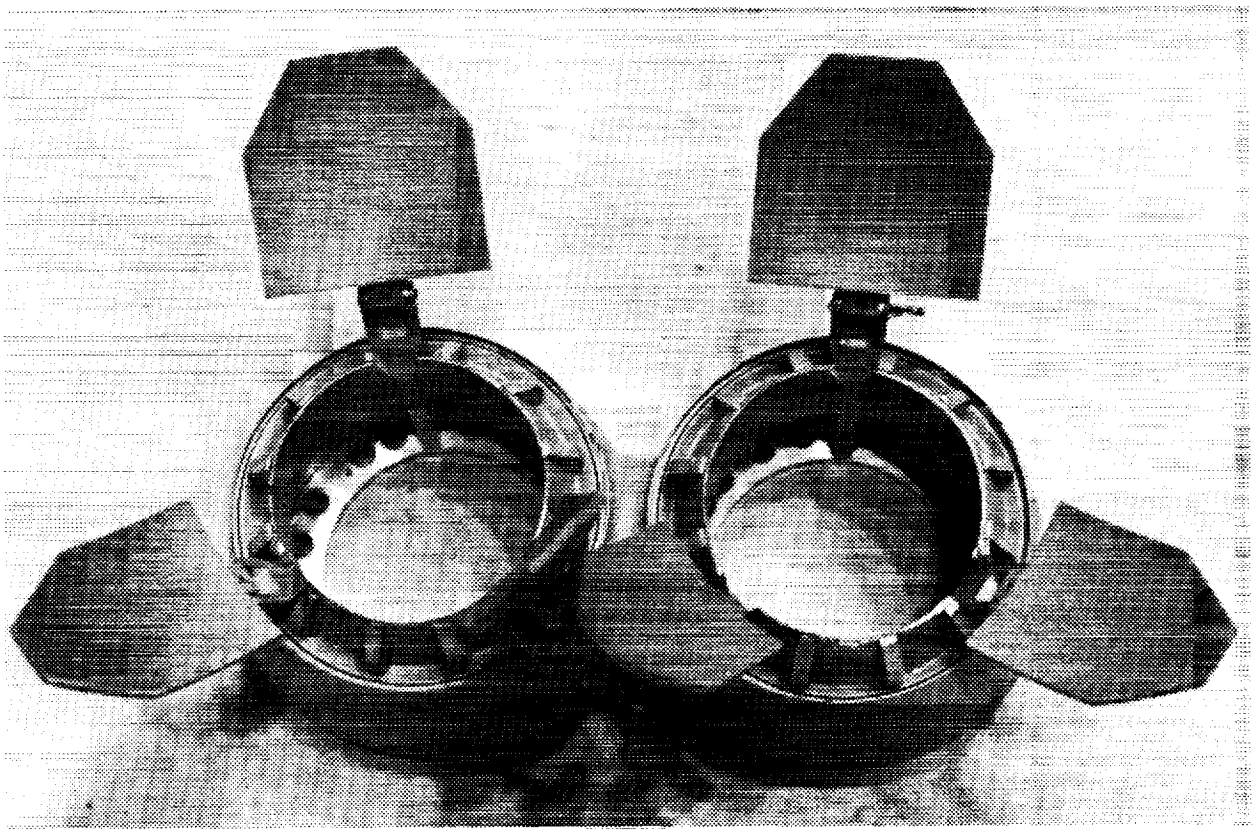

Fig. 7 Closeup of exhaust nozzles and vanes used on F/A-18 HARV TVCS 16-percent scale model.

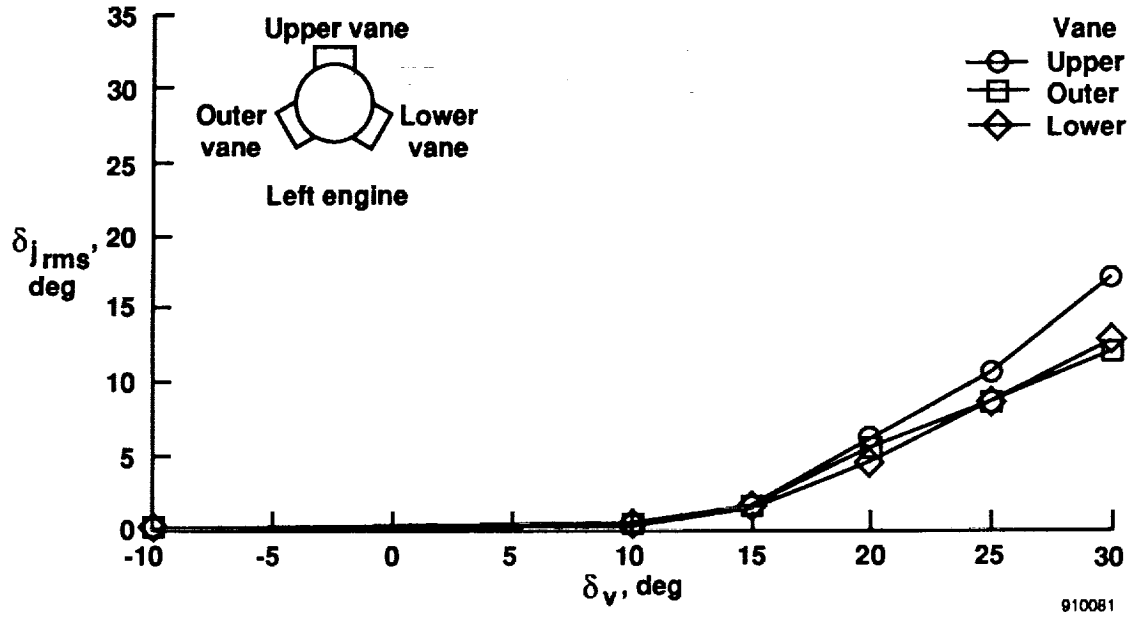

Fig. 8 Jet deflection turning angle as a function of single-vane deflection for all three vanes. With the military power nozzle and NPR = 2.

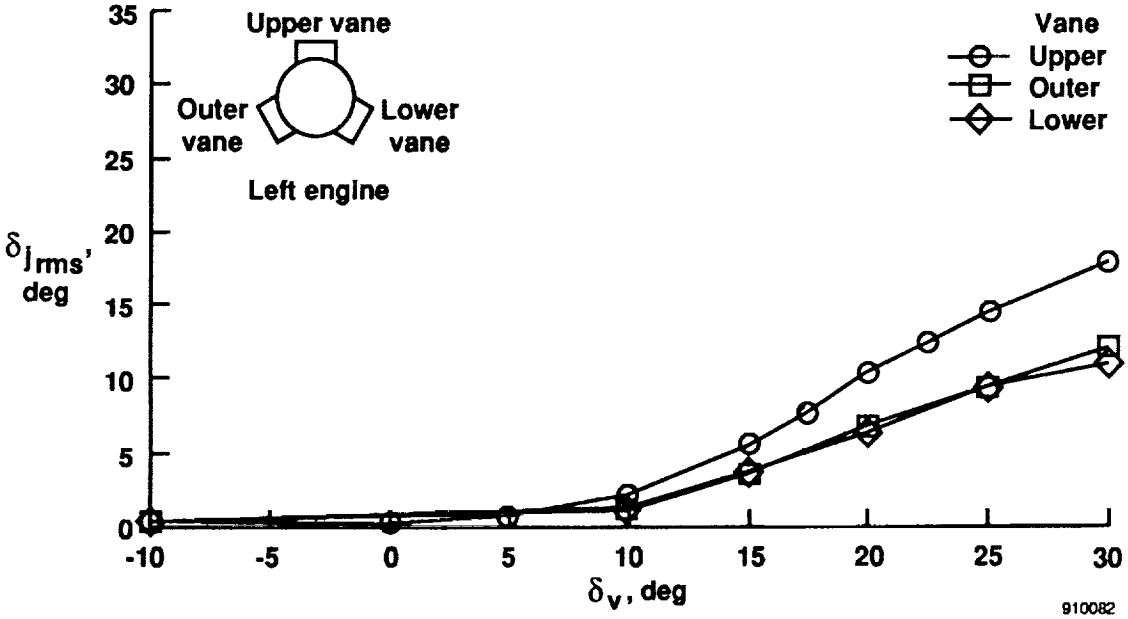

Fig. 9 Jet deflection turning angle as a function of single-vane deflection for all three vanes. With the maximum afterburner nozzle and NPR = 2.

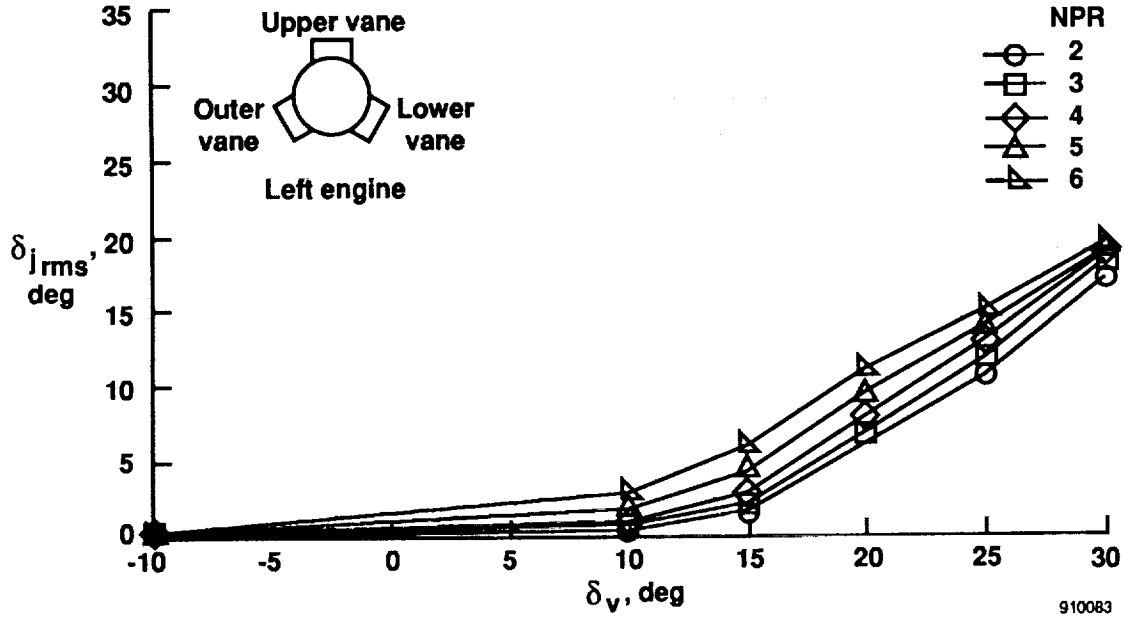

Fig. 10 Jet deflection turning angle as a function of single-vane deflection (upper) and varying NPR. With the military power nozzle.

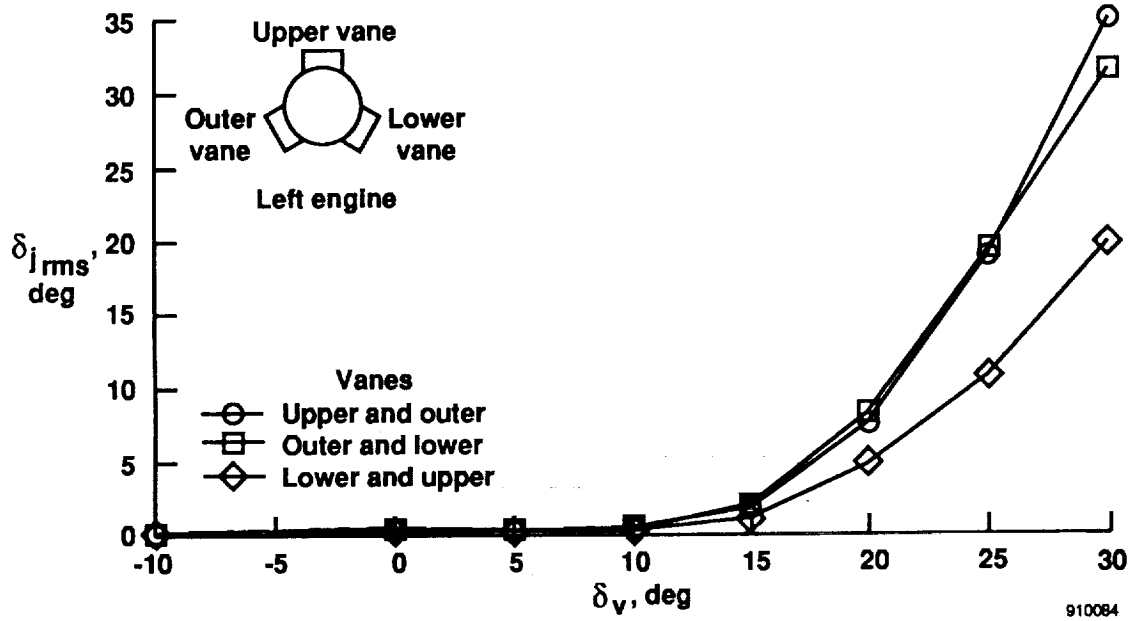

Fig. 11 Jet deflection turning angle as a function of two-vane equal deflections for all two-vane combinations. With the military power nozzle and NPR = 2.

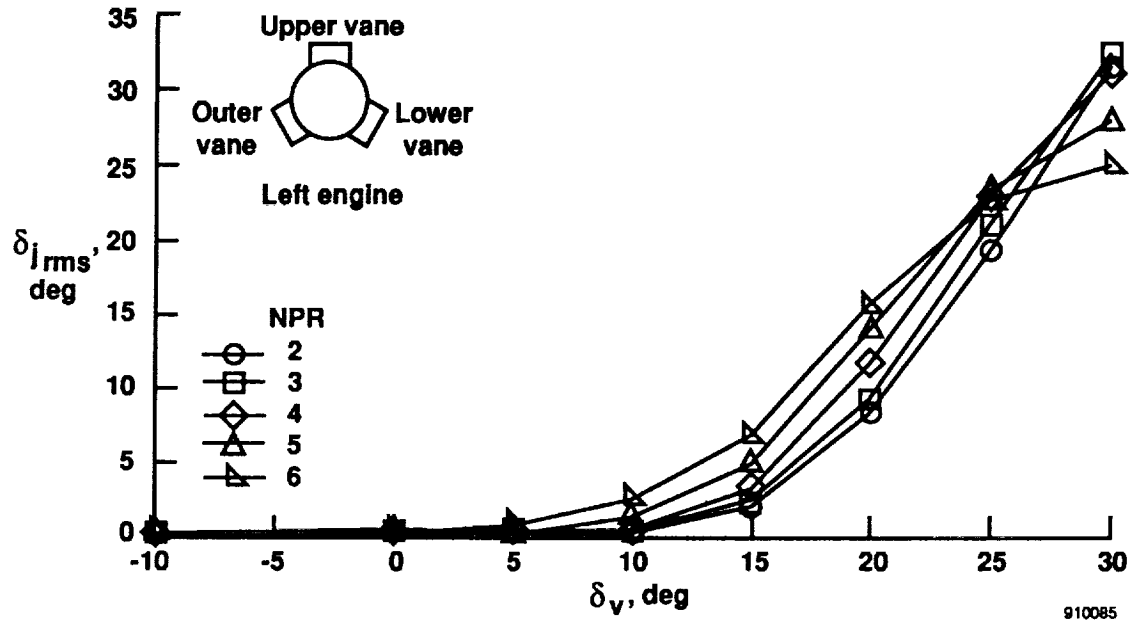

Fig. 12 Jet deflection turning angle as a function of two-vane equal deflections (outer and lower), with varying NPR. With the military power nozzle.

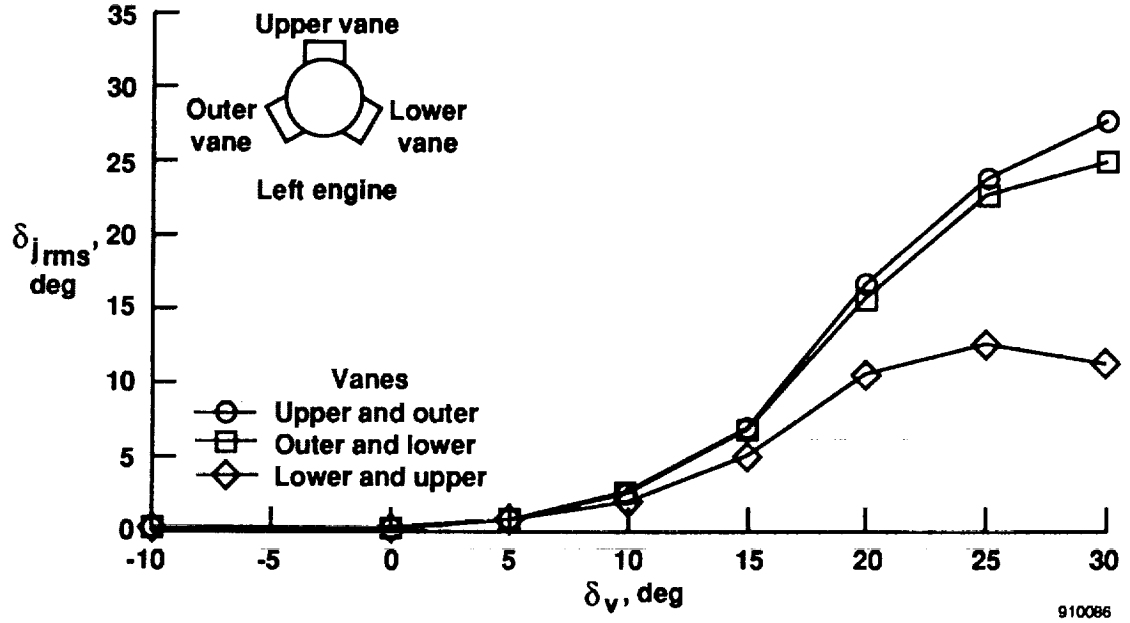

Fig. 13 Jet deflection turning angle as a function of two-vane equal deflections for all two-vane combinations. With the military power nozzle and NPR = 6 showing retracted vane interference.

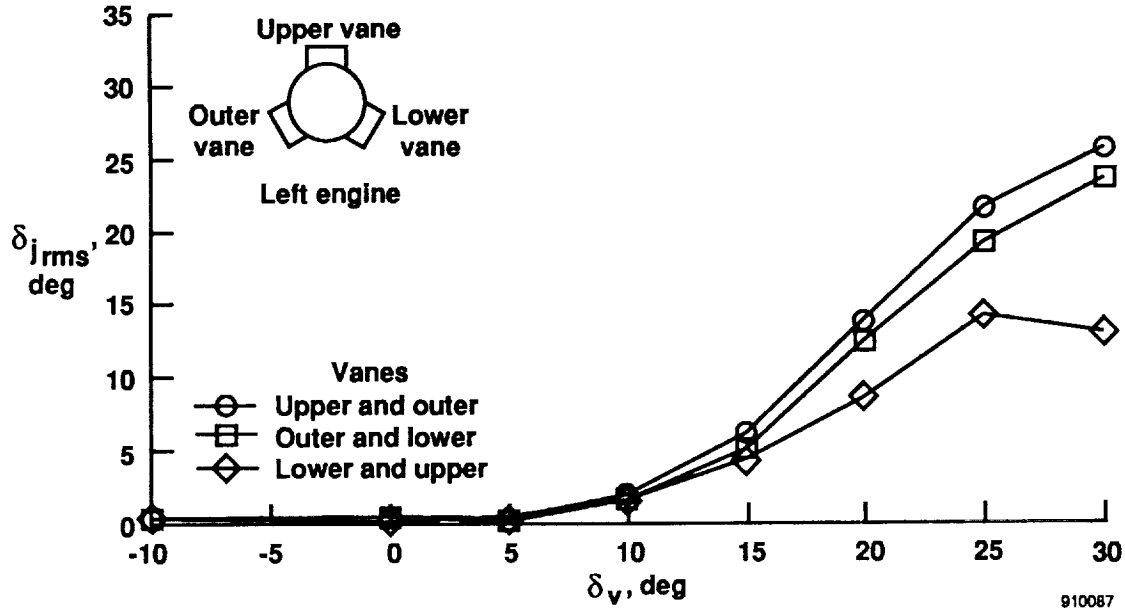

Fig. 14 Jet deflection turning angle as a function of two-vane equal deflections for all two-vane combinations. With the maximum afterburner nozzle and NPR = 2.

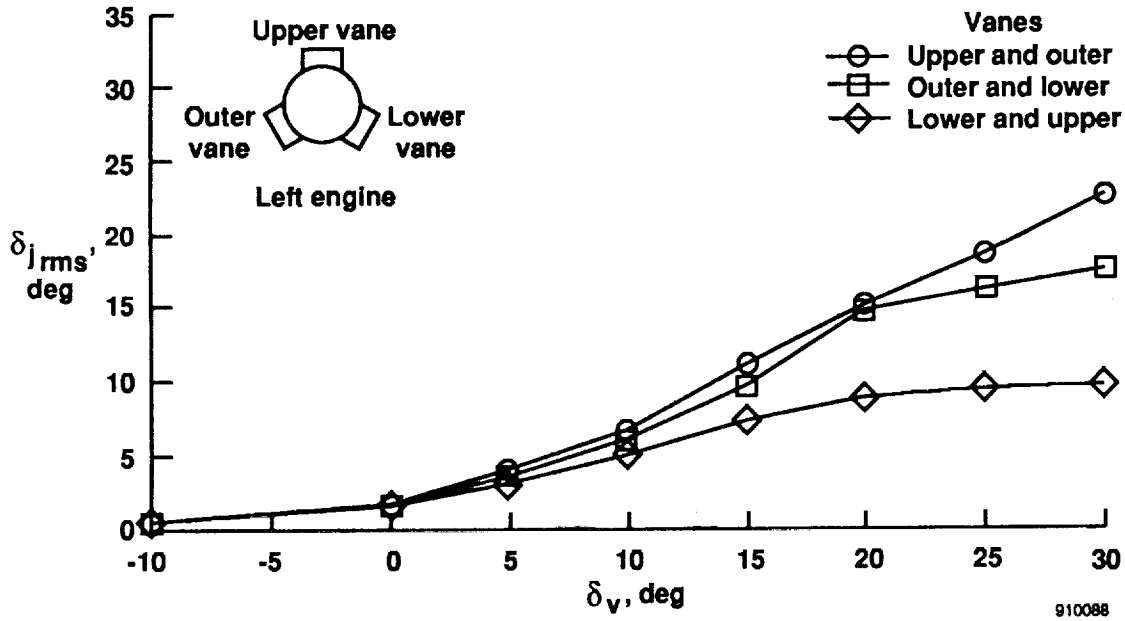

Fig. 15 Jet deflection turning angle as a function of two-vane equal deflections for all two-vane combinations. With the maximum afterburner nozzle and NPR = 6 showing retracted vane interference.

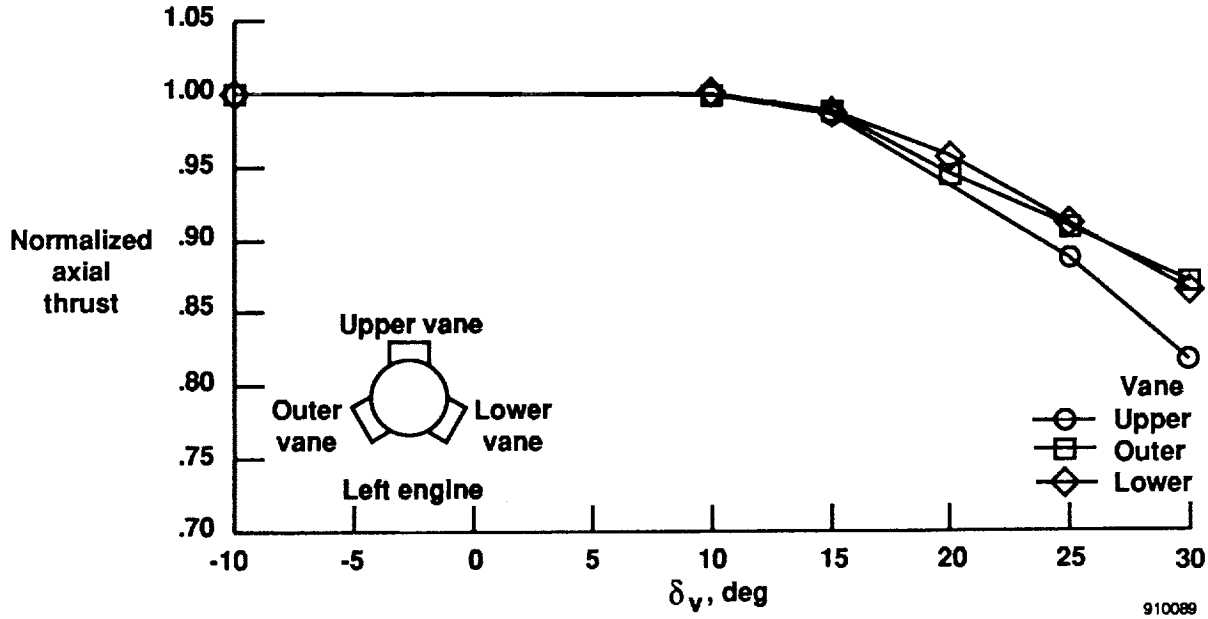

Fig. 16 Normalized axial force thrust loss as a function of vane deflection angle for all single-vane deflections. With the military power nozzle and NPR = 2.

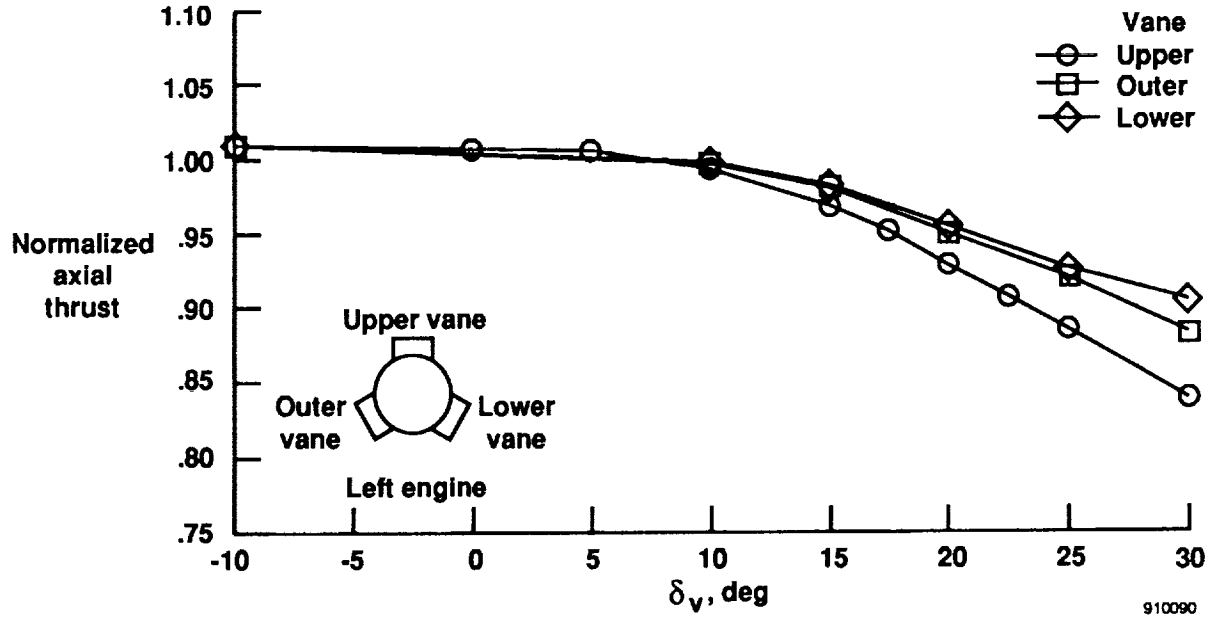

Fig. 17 Normalized axial force thrust loss as a function of vane deflection angle for all single-vane deflections. With the maximum afterburner nozzle and NPR = 2.

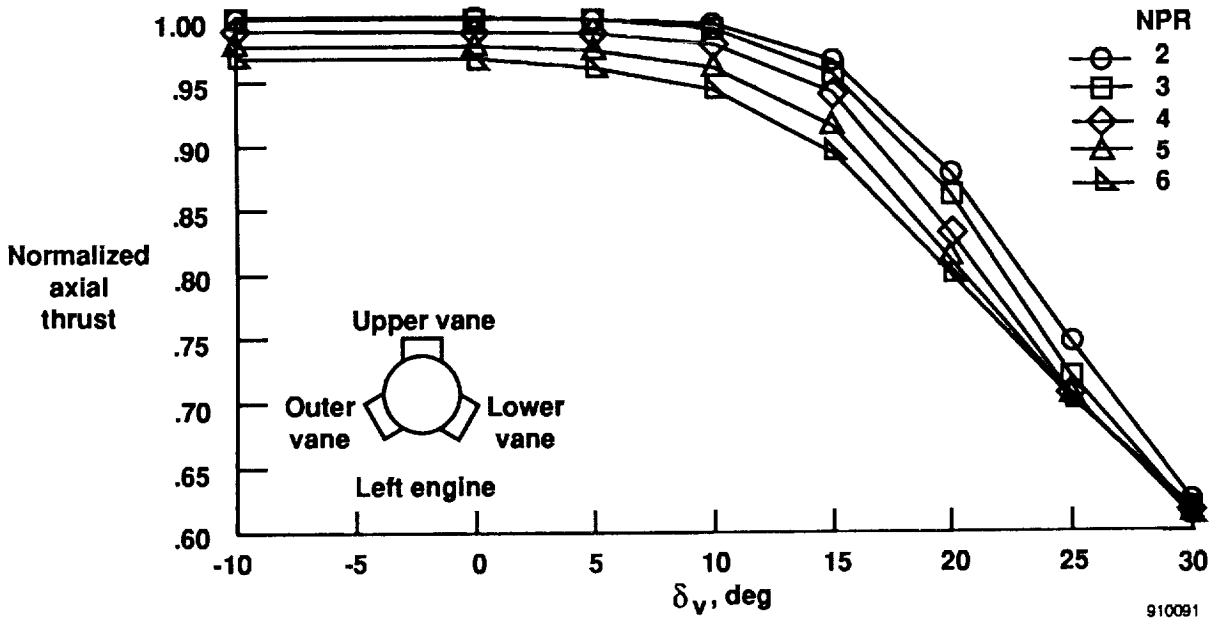

Fig. 18 Normalized axial force thrust loss as a function of a two-vane equal deflections (outer and lower) with varying NPR. With the military power nozzle.

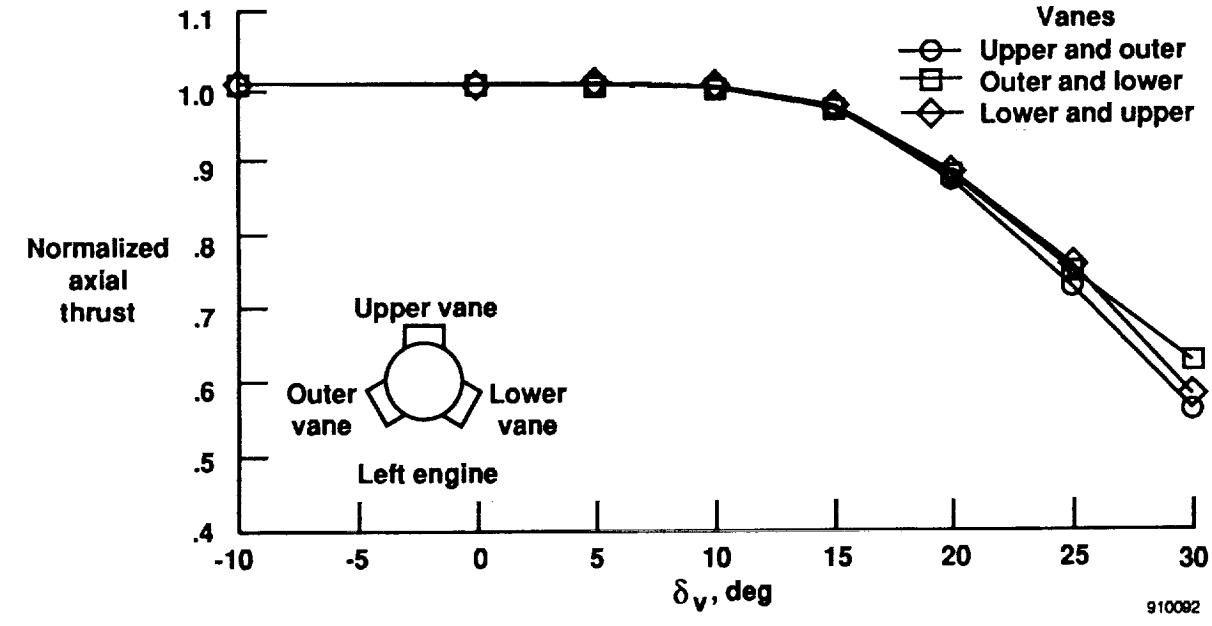

Fig. 19 Normalized resultant force thrust loss as a function of a two-vane deflections for all two-vane equal deflection combinations, NPR = 2.

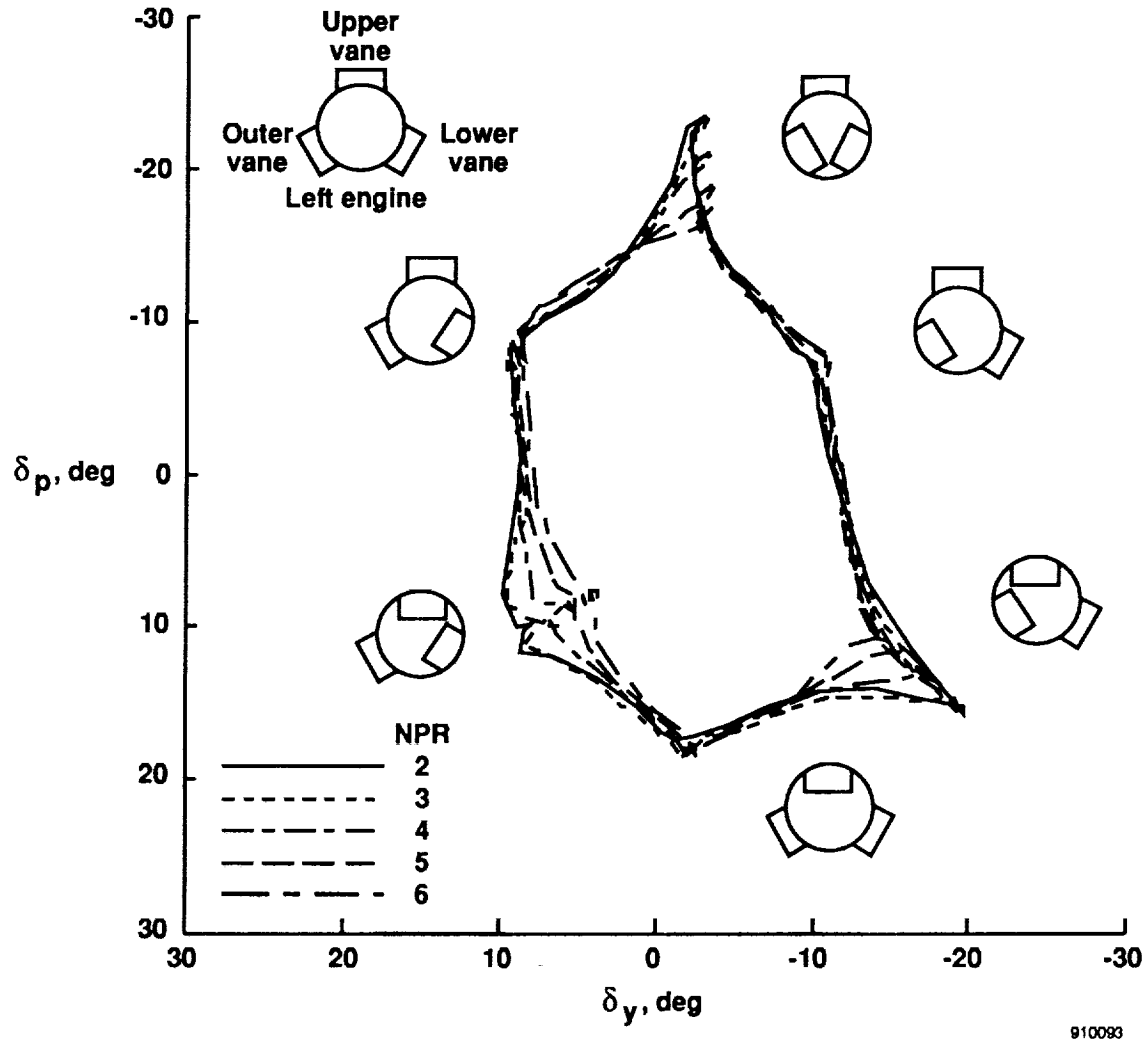

Fig. 20 Maximum jet deflection turning angle envelope, in pitch and yaw, where at least one vane is deflected 30°. Maximum afterburner nozzle and varying NPR showing retracted vane interference near corners with two-vane equal deflections. Symbols omitted for clarity.

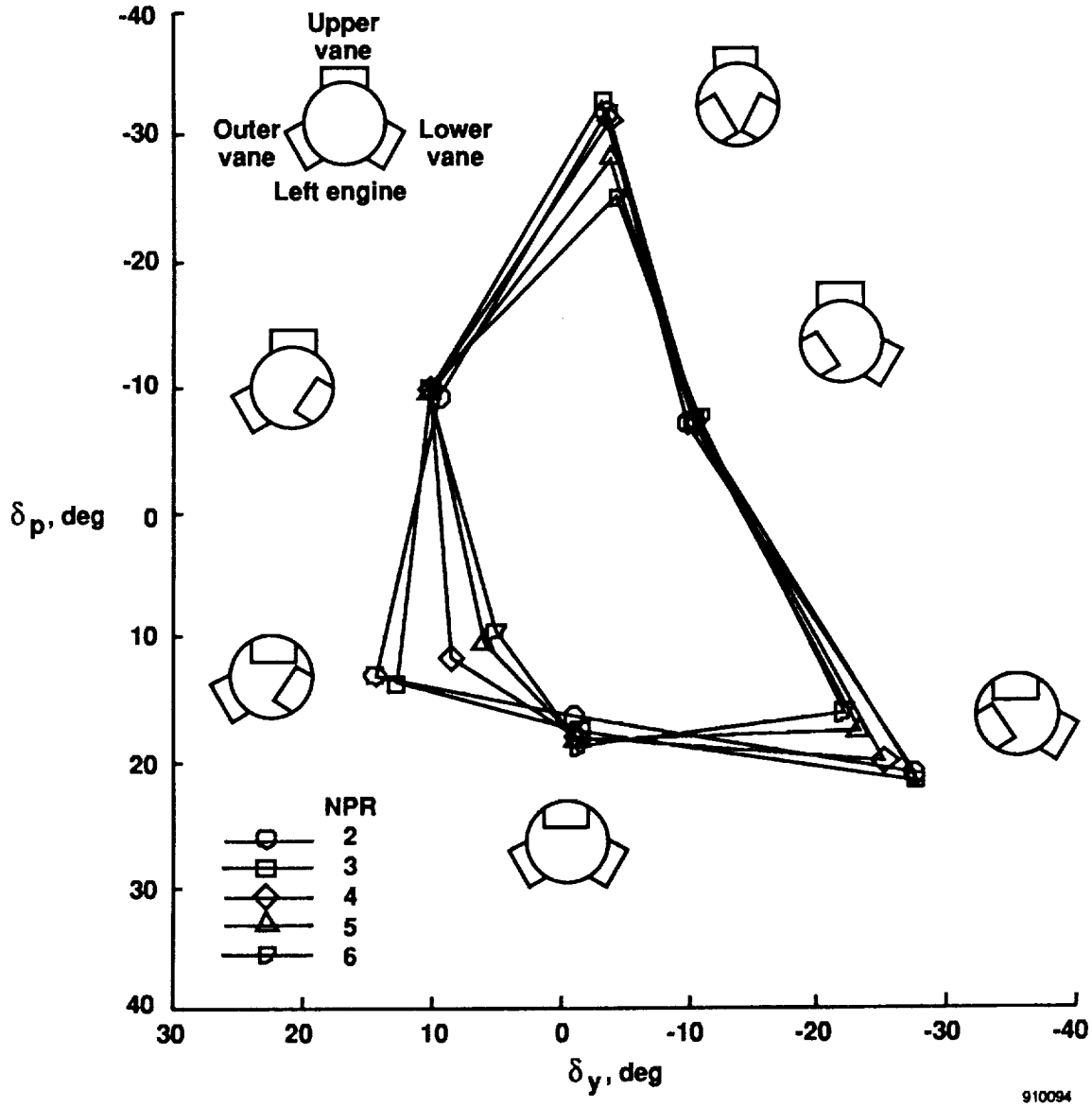

Fig. 21 Maximum jet deflection turning angle envelope, in pitch and yaw, where at least one vane is deflected 30°. Military power nozzle and varying NPR showing retracted vane interference near corners with two-vane equal deflections.

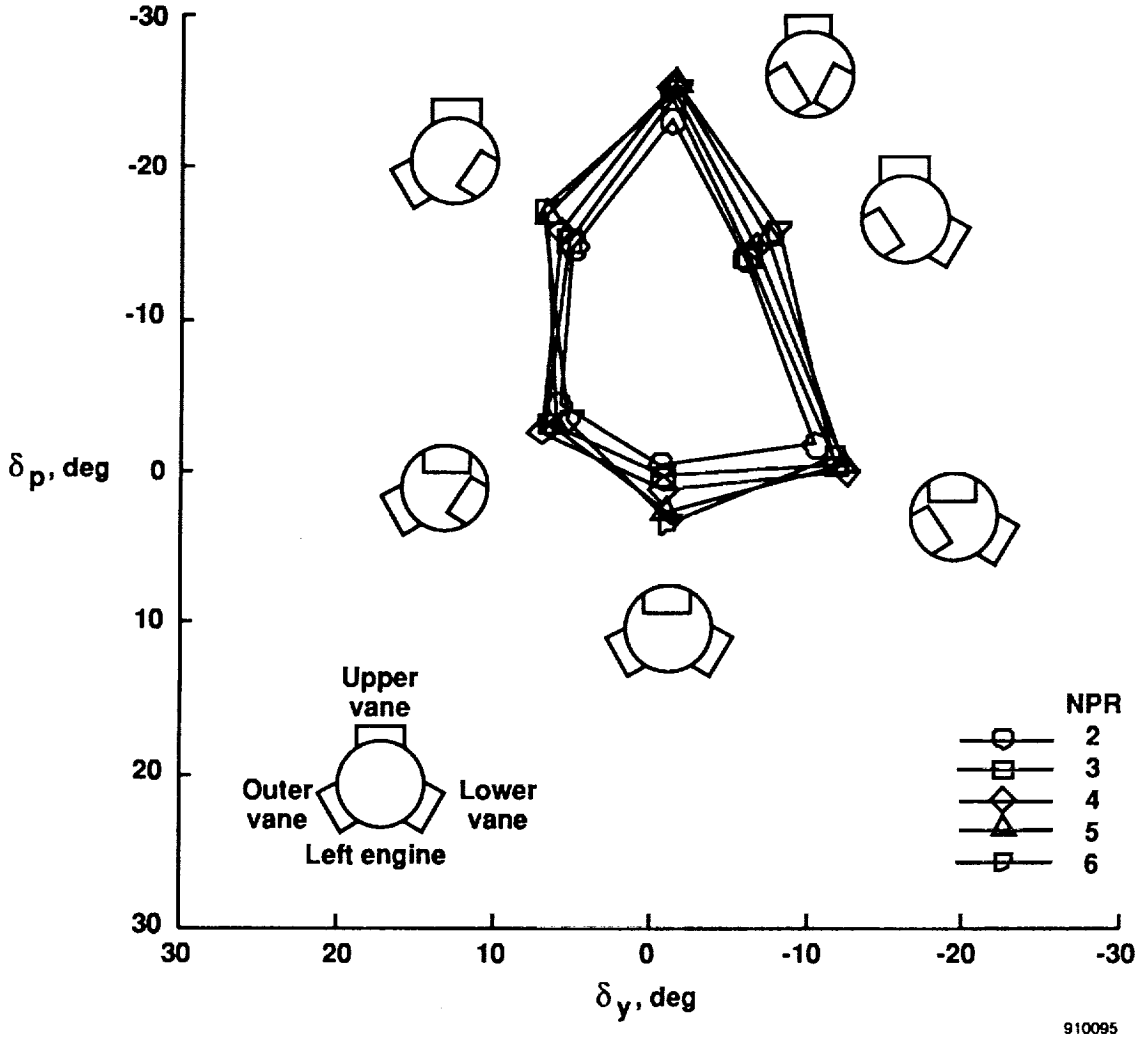

Fig. 22 Maximum jet deflection turning angle envelope, in pitch and yaw, where at least one vane is deflected 20°. With the military power nozzle and varying NPR showing lack of retracted vane interference near corners with two-vane equal deflections.

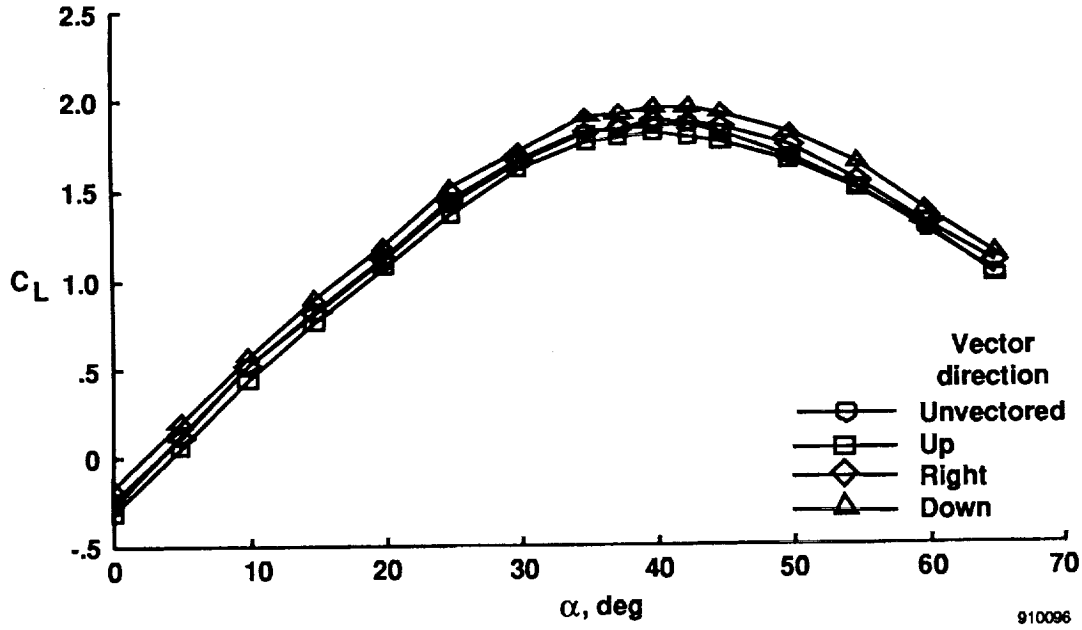

Fig. 23 Lift coefficient as a function of angle of attack, with thrust vectoring varying direction. $\delta_{lef} = 34°$, $\delta_{tef} = 0°$, $\delta_e = -12°$, $\delta_a = 0°$, $\delta_r = 0°$, and $C_t = 0.8$.

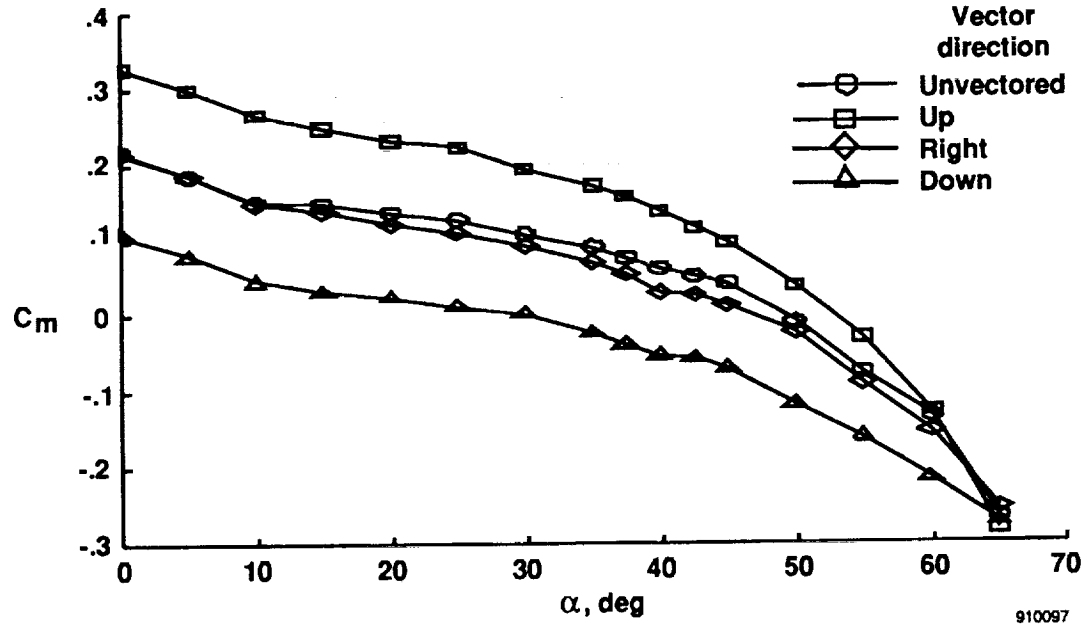

Fig. 24 Pitching moment coefficient as a function of angle of attack, with thrust vectoring varying direction. $\delta_{lef} = 34°$, $\delta_{tef} = 0°$, $\delta_e = -12°$, $\delta_a = 0°$, $\delta_r = 0°$, and $C_t = 0.8$.

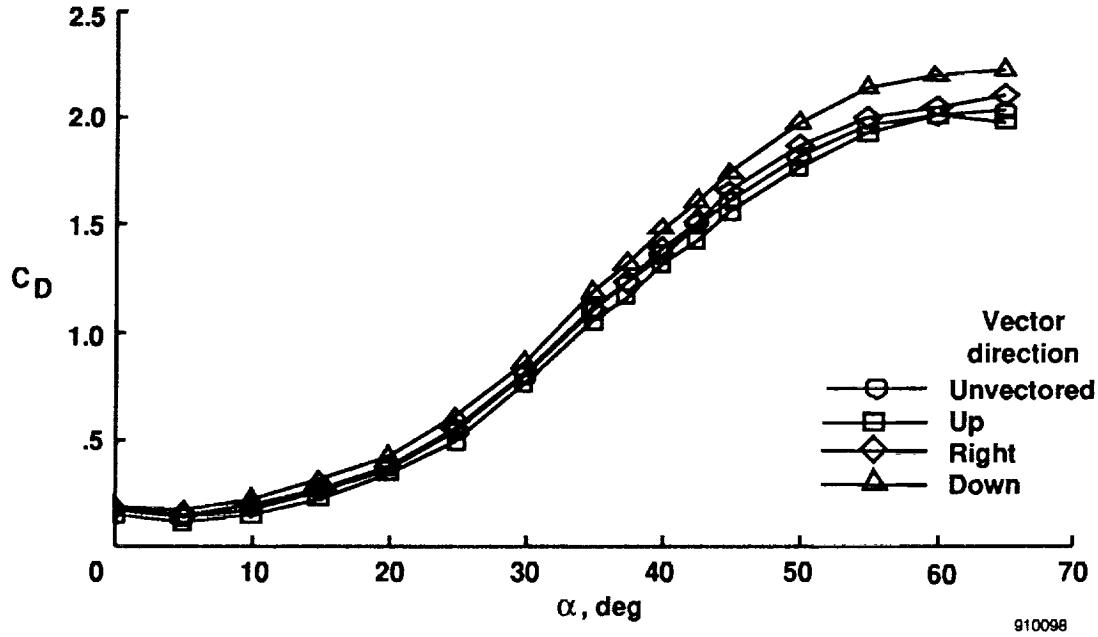

Fig. 25 Drag coefficient as a function of angle of attack, with thrust vectoring varying direction. $\delta_{lef} = 34°$, $\delta_{tef} = 0°$, $\delta_e = -12°$, $\delta_a = 0°$, $\delta_r = 0°$, and $C_t = 0.8$.

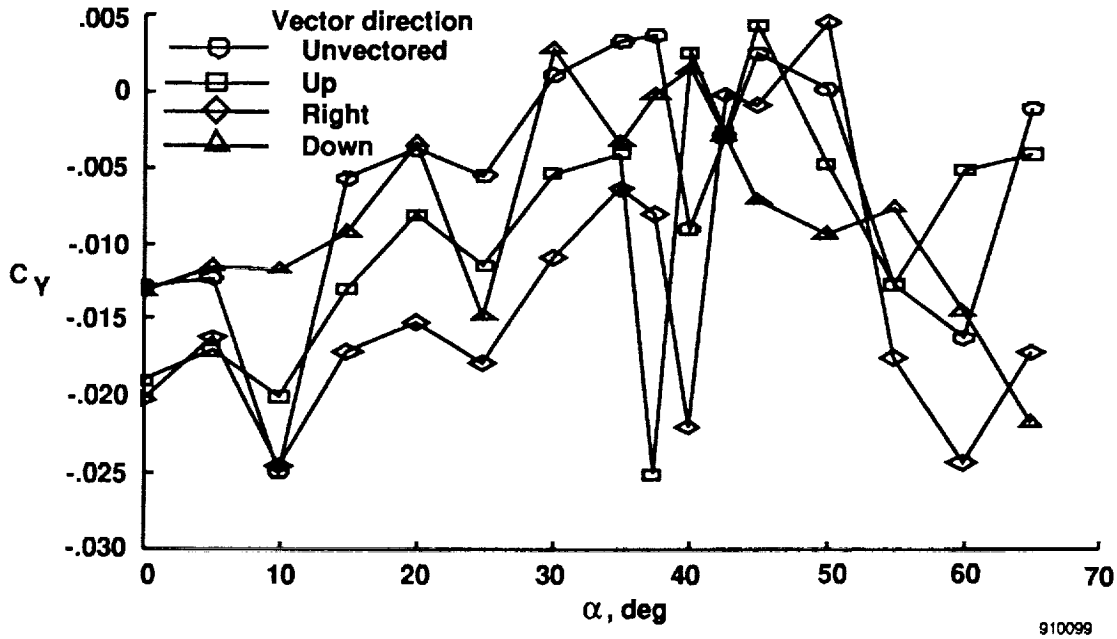

Fig. 26 Side force coefficient as a function of angle of attack, with thrust vectoring varying direction. $\delta_{lef} = 34°$, $\delta_{tef} = 0°$, $\delta_e = -12°$, $\delta_a = 0°$, $\delta_r = 0°$, and $C_t = 0.8$.

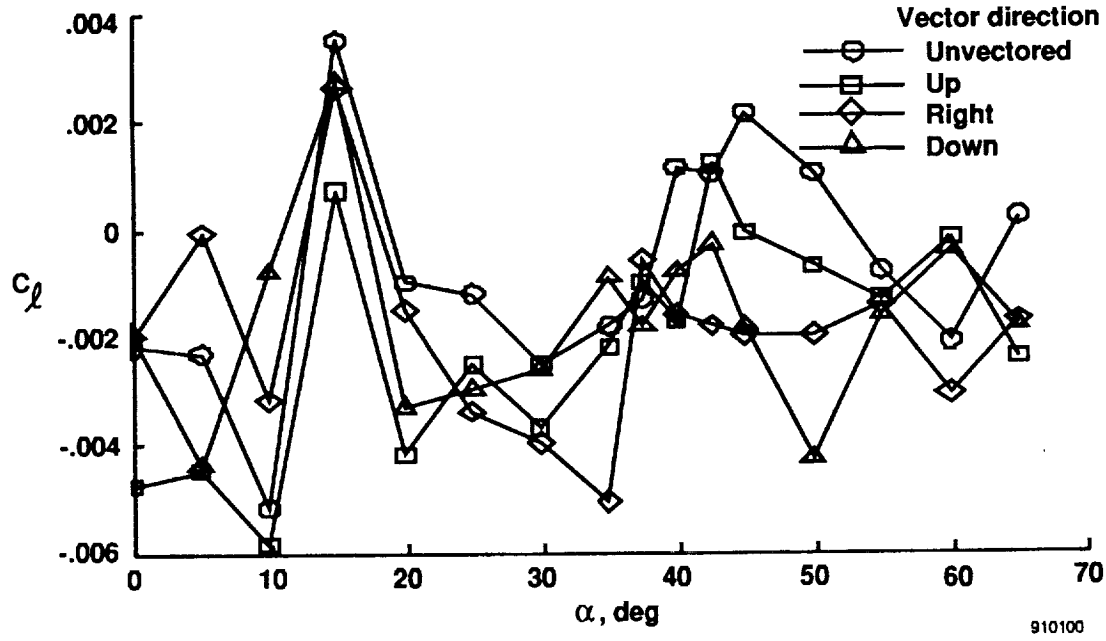

Fig. 27 Rolling moment coefficient as function of angle of attack, with thrust vectoring varying direction. $\delta_{\ell ef} = 34°$, $\delta_{tef} = 0°$, $\delta_e = -12°$, $\delta_a = 0°$, $\delta_r = 0°$, and $C_t = 0.8$.

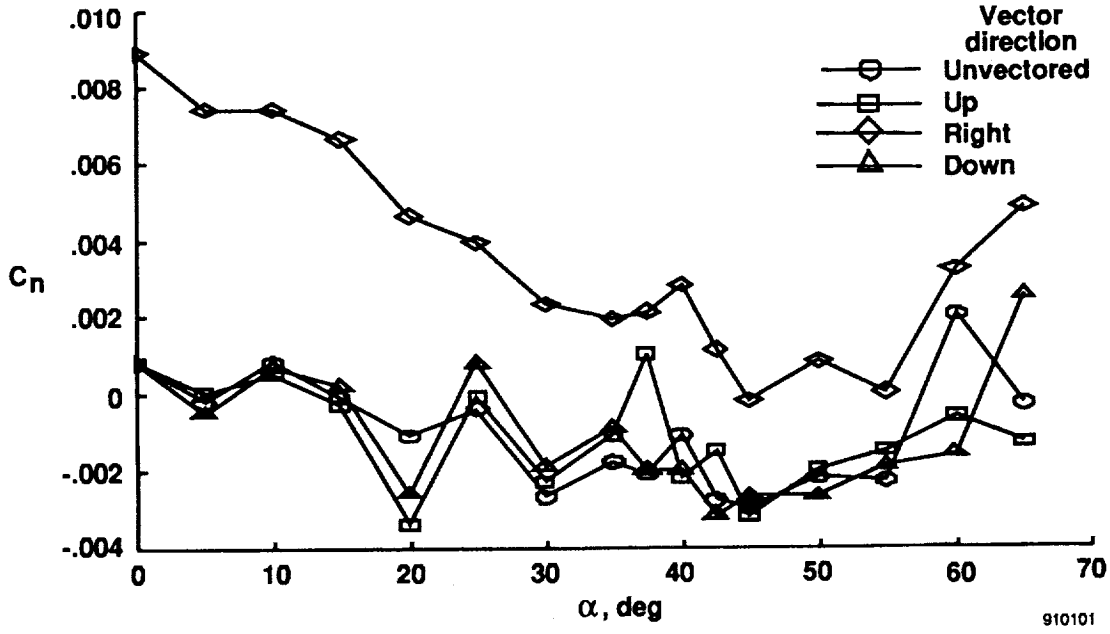

Fig. 28 Yawing moment coefficient as a function of angle of attack, with thrust vectoring varying direction. $\delta_{\ell ef} = 34°$, $\delta_{tef} = 0°$, $\delta_e = -12°$, $\delta_a = 0°$, $\delta_r = 0°$, and $C_t = 0.8$.

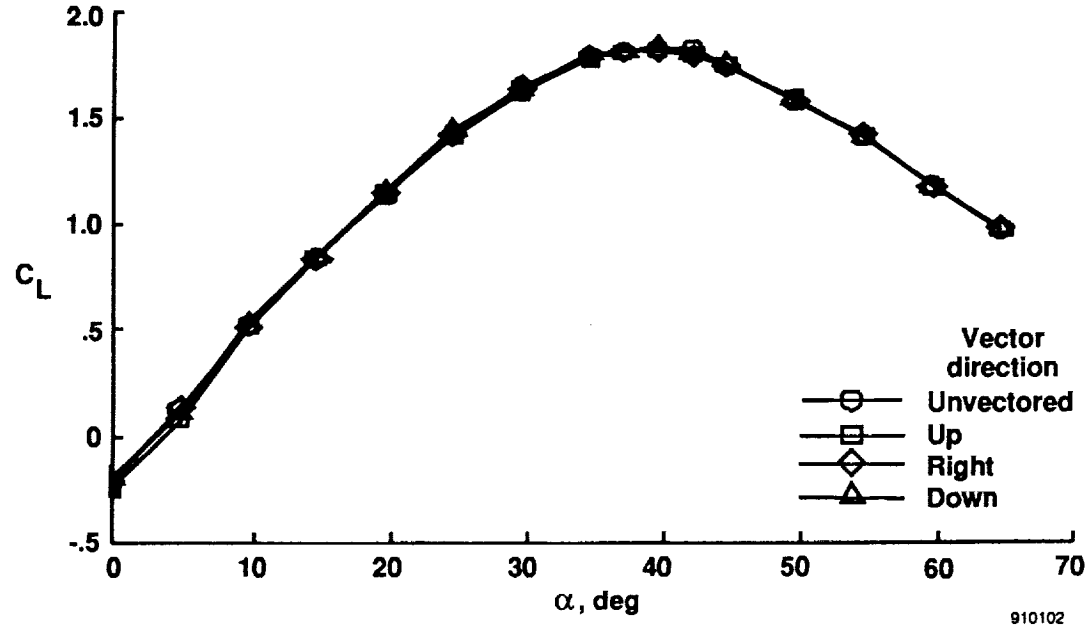

Fig. 29 Lift coefficient as a function of angle of attack, with thrust vectoring vanes set to varying directions and no thrust. $\delta_{lef} = 34°$, $\delta_{tef} = 0°$, $\delta_e = -12°$, $\delta_a = 0°$, and $\delta_r = 0°$.

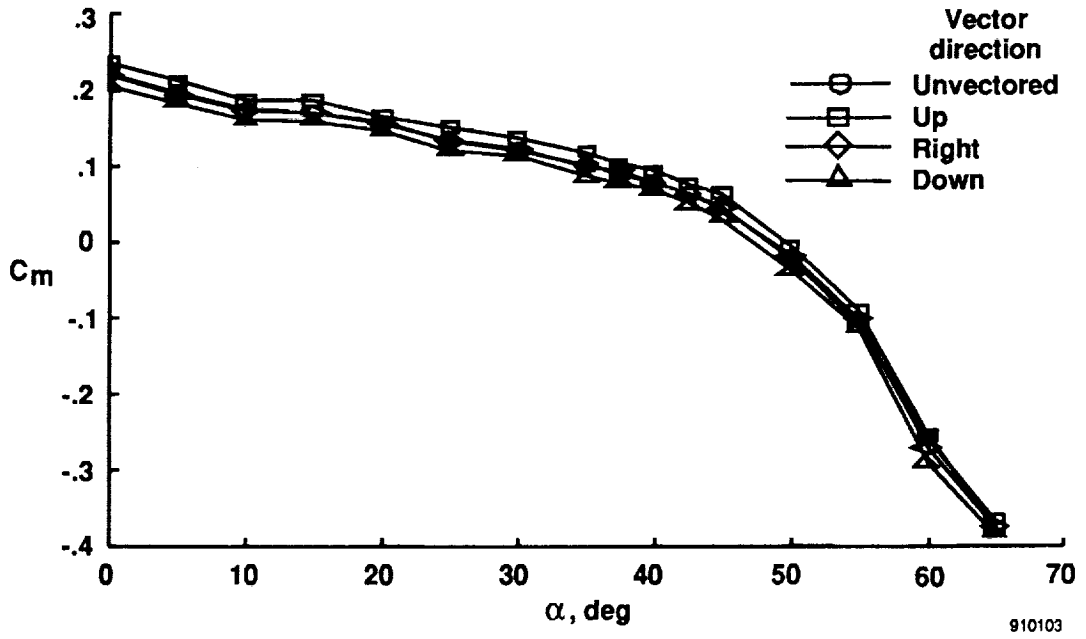

Fig. 30 Pitching moment coefficient as a function of angle of attack, with thrust vectoring vanes set to varying directions and no thrust. $\delta_{lef} = 34°$, $\delta_{tef} = 0°$, $\delta_e = -12°$, $\delta_a = 0°$, and $\delta_r = 0°$.

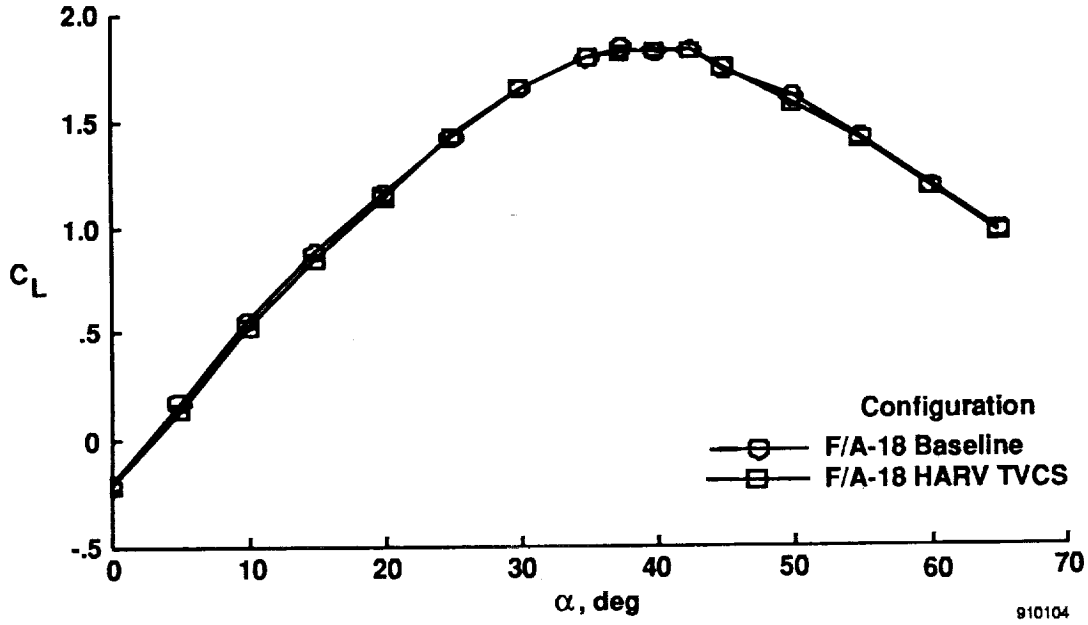

Fig. 31 Lift coefficient as a function of angle of attack, with TVCS installed compared to baseline F/A-18 (no TVCS installed) and no thrust. $\delta_{\ell ef} = 34°$, $\delta_{tef} = 0°$, $\delta_e = -12°$, $\delta_a = 0°$, and $\delta_r = 0°$.

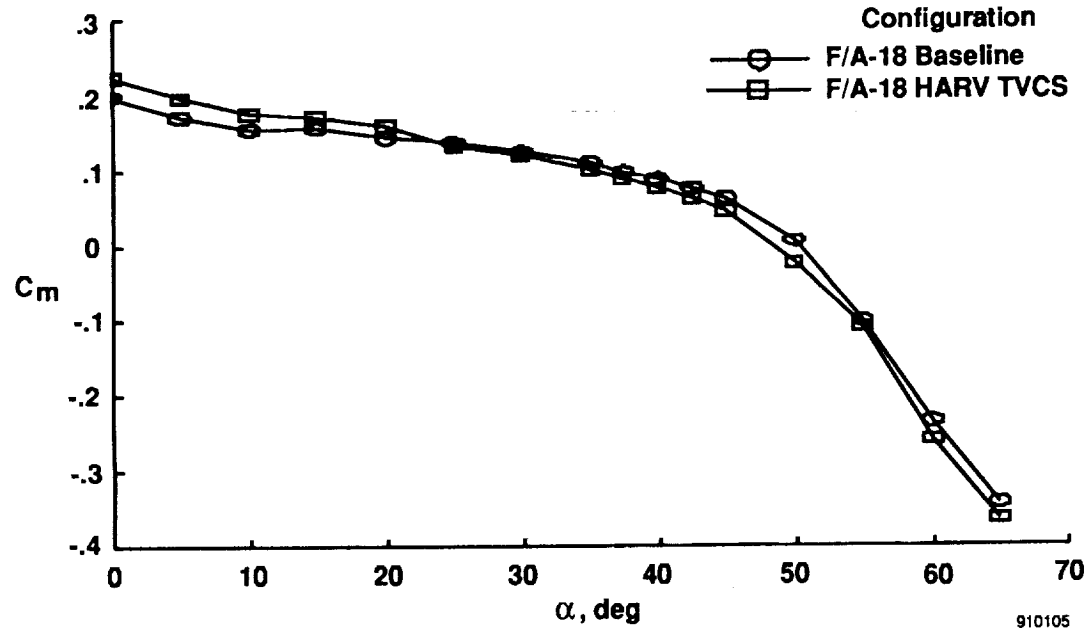

Fig. 32 Pitching moment coefficient as a function of angle of attack, with TVCS installed compared to baseline F/A-18 (no TVCS intalled) and no thrust. $\delta_{\ell ef} = 34°$, $\delta_{tef} = 0°$, $\delta_e = -12°$, $\delta_a = 0°$, and $\delta_r = 0°$.

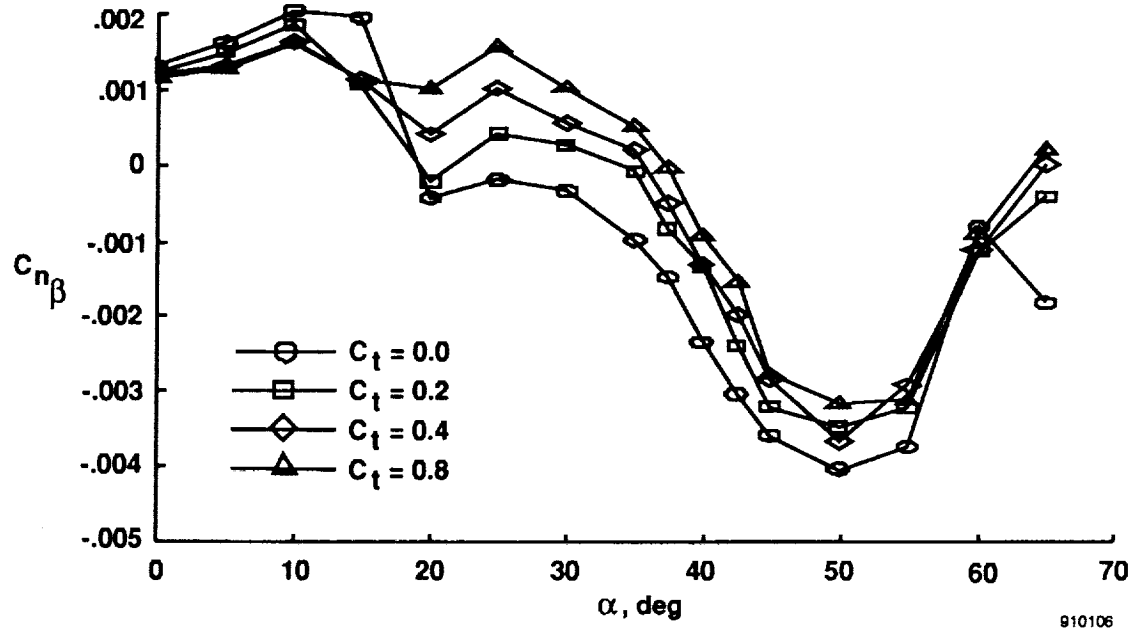

Fig. 33 Linearized yawing moment coefficient with angle of sideslip, at $-4°$ and $4°$, as a function of angle of attack, with varying thrust coefficient, with TVCS installed. $\delta_{lef} = 34°$, $\delta_{tef} = 0°$, $\delta_e = -12°$, $\delta_a = 0°$, and $\delta_r = 0°$.

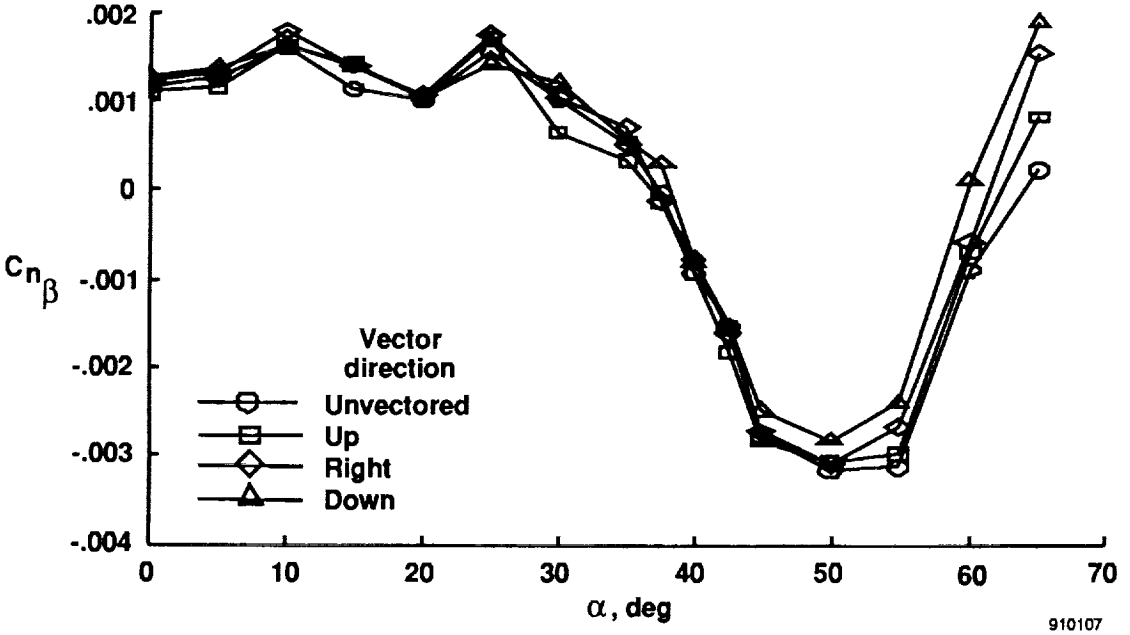

Fig. 34 Linearized yawing moment coefficient with angle of sideslip, at $-4°$ and $4°$, as a function of angle of attack, with varying vectoring directions. $\delta_{lef} = 34°$, $\delta_{tef} = 0°$, $\delta_e = -12°$, $\delta_a = 0°$, $\delta_r = 0°$, and $C_t = 0.8$.

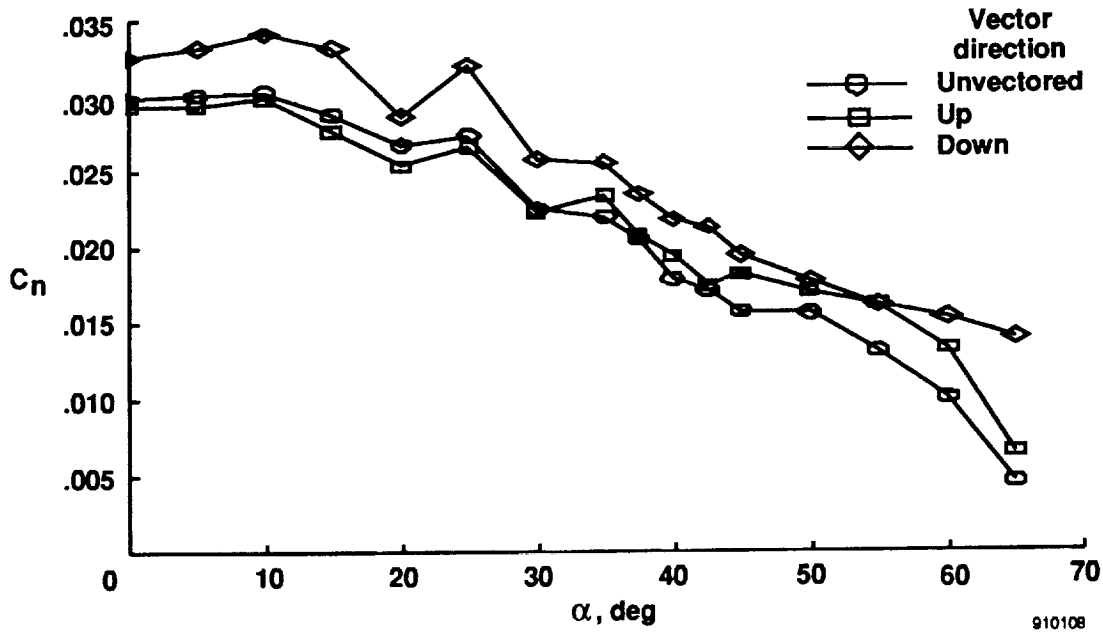

Fig. 35 Yawing moment coefficient as a function of angle of attack, with varying vectoring directions and rudders set to 30°. $\delta_{lef} = 34°$, $\delta_{tef} = 0°$, $\delta_e = -12°$, $\delta_a = 0°$, and $C_t = 0.8$.

NASA
National Aeronautics and Space Administration

Report Documentation Page

1. Report No.	2. Government Accession No.	3. Recipient's Catalog No.
NASA TM-101741		

4. Title and Subtitle

Multiaxis Thrust Vectoring Using Axisymmetric Nozzles and Postexit Vanes on an F/A-18 Configuration Vehicle

5. Report Date
April 1991

6. Performing Organization Code

7. Author(s)
Albion H. Bowers, Gregory K. Noffz (Dryden Flight Research Facility, Edwards, California) Sue B. Grafton, Mary L. Mason (Langley Research Center, Hampton, Virginia) Lee R. Peron (California Polytechnic State University, San Luis Obispo, California)

8. Performing Organization Report No.
H-1705

10. Work Unit No.
RTOP 533-02-01

9. Performing Organization Name and Address
NASA Dryden Flight Research Facility
P.O. Box 273
Edwards, California 93523-0273

11. Contract or Grant No.

13. Type of Report and Period Covered
Technical Memorandum

12. Sponsoring Agency Name and Address
National Aeronautics and Space Administration
Washington, DC 20546-3191

14. Sponsoring Agency Code

15. Supplementary Notes

Prepared for presentation at the High-Angle-of-Attack Technology Conference, NASA Langley Research Center, Hampton, Virginia, October 30–November 1, 1990.

16. Abstract

A ground-based investigation was conducted on an operational system of multiaxis thrust vectoring using postexit vanes around an axisymmetric nozzle. This thrust vectoring system will be tested on the NASA F/A-18 High Alpha Research Vehicle (HARV) aircraft. The system provides thrust vectoring capability in both pitch and yaw. Ground-based data were gathered from two separate tests at NASA Langley Research Center. The first was a static test in the 16-ft Transonic Tunnel Cold-Jet Facility with a 14.25-percent scale model of the axisymmetric nozzle and the postexit vanes. The second test was conducted in the 30- by 60-ft wind tunnel with a 16-percent F/A-18 complete configuration model. Data from the two tests are being used to develop models of jet plume deflection and thrust loss as a function of vane deflection. In addition, an aerodynamic interaction model based on plume deflection angles will be developed. Results from the scale model nozzle test showed that increased vane deflection caused increased exhaust plume turning. Aerodynamic interaction effects consisted primarily of favorable interaction of moments and unfavorable interaction of forces caused by the vectored jet plume.

17. Key Words (Suggested by Author(s))	18. Distribution Statement
Aerodynamics High angle of attack Thrust vectoring	Unclassified — Unlimited Subject category 02

19. Security Classif. (of this report)	20. Security Classif. (of this page)	21. No. of Pages	22. Price
Unclassified	Unclassified	36	A03

For sale by the National Technical Information Service, Springfield, Virginia 22161-2171